NATIONAL AERONAUTICS AND SPACE ADMINISTRATION

Technical Report 32-1161

Mariner Venus 67 Structural Developmental and Qualification Vibration Test Report

R. E. Freeland

JET PROPULSION LABORATORY
CALIFORNIA INSTITUTE OF TECHNOLOGY
PASADENA, CALIFORNIA
November 1, 1967

NATIONAL AERONAUTICS AND SPACE ADMINISTRATION

JPL - ~~Technical~~ Report 32-1161

Mariner Venus 67 Structural Developmental and Qualification Vibration Test Report

R. E. Freeland

Approved by:

M. E. Alper

M. E. Alper, *Manager*
Applied Mechanics Section

JET PROPULSION LABORATORY
CALIFORNIA INSTITUTE OF TECHNOLOGY
PASADENA, CALIFORNIA

November 1, 1967

TECHNICAL REPORT 32-1161

Prepared Under Contract No. NAS 7-100
National Aeronautics & Space Administration

Acknowledgment

The author is indebted to Dr. M. R. Trubert, member of the Technical Staff of the Jet Propulsion Laboratory Applied Mechanics Section, for the derivation of the multi-frequency torsional transient load requirements (Appendix C), the implementation of these loads to the test structure, and the torsional data analysis and its interpretation.

Thanks are also extended to three other Applied Mechanics Section contributors: to R. Bamford, member of the Technical Staff, for the comparison of his solar panel analysis to test data; to J. R. Chisholm, development engineer, for interpretation of the test data for the high-gain antenna; and to W. W. Edwards, test engineer, for his help in implementation of the test and data reduction.

Special mention is made of the Environmental and Dynamic Testing Section for the fine execution of the test, and of the Data Analysis Laboratory, Data Systems Section, for data reduction.

Contents

Tables

Contents (contd)

Figures

Contents (contd)

Figures (contd)

Abstract

This report describes the structural developmental forced-vibration test program accomplished on the *Mariner V* structural test model. Data included are concerned with sine-wave excitation from 5 to 200 Hz along lateral and axial axes of the spacecraft, and with modulated sine and multifrequency pulse-type excitation introduced torsionally. Implementation of dynamic test loads and supporting instrumentation, data recording, and analysis are discussed. Dynamic response characteristics of major substructures are evaluated with respect to structural integrity and correlation to structural analysis; this includes the pressure-dependent response of the post-injection propulsion system and the response of the tip-latched and viscous-damped solar panels. The effect of spacecraft elastic torsional response when subjected to modulated sine wave excitation, as compared with multifrequency transient excitation, is discussed. Test data verified the *Mariner V* to be structurally adequate to satisfy mission objectives.

Mariner Venus 67 Structural Developmental and Qualification Vibration Test Report

I. Introduction

Initial structural developmental vibration testing of the *Mariner* Venus 67 was conducted during July and August 1966. Qualification testing was performed with the structural test model (STM), there being no proof test model (PTM) available for such. Although tests were accomplished in the frequency range of 5 to 2000 Hz, this report presents only the data for the basic structural response in the range from 5 to 200 Hz; high-frequency and complex-wave test data will be presented in another document.

Peculiar to the first test series were torsional excitation tests that included testing of one flight-type, multicelled solar panel and of the post-injection propulsion-system (PIPS) pressure configuration. The objectives of this series were the following:

(1) To determine dynamic-response characteristics of the STM for the input loads defined in JPL specifications.[1]

(2) To determine the adequacy of the primary structure when subjected to qualification dynamic loads.

(3) To determine the effect of the PIPS fuel/pressure configuration on dynamic response characteristics of spacecraft.

(4) To evaluate the performance of the new equalization equipment for its application to flight acceptance (FA) testing at the system level.

(5) To qualify one, celled, solar panel at the system level.

In November 1966, follow-up developmental vibration testing was conducted to obtain supplemental dynamic-response data required by design changes and, also, to qualify structural hardware not included in the first STM test. Tests runs common to both of the series were implemented and performed in like manner. Modified hardware of the first test was used in the follow-up tests. There were four purposes for conducting the second test series:

(1) To obtain supplemental dynamic-response data required by recent design changes of the *Mariner* V STM for input loads as described in the JPL specifications cited in footnote 1.

(2) To determine the adequacy of the modified *Mariner* V primary structure and the structural components when subjected to structural qualification dynamic loads.

[1] "Test Specification *Mariner* Venus 67 Structural and Environmental Vibration Qualification Test Requirements," JPL Spec MVB 50587-TST, Jet Propulsion Laboratory, Pasadena, California, June 27, 1966; and "Test Specification *Mariner* Venus 67 System Level Solar Panel Qualification Testing," JPL Spec MVP-50602-TST, July 28, 1966. (Specifications are available to qualified requesters.)

(3) To qualify structural hardware which either was not included on the previous STM or had been modified since the previous tests.

(4) To verify complex-wave vibration-control equipment operational procedure to be used on flight spacecraft testing.

II. Test Program

A. Structural Test Model and Adapter

All major assemblies comprising the structural test model were flight-type hardware whenever possible. Mockups of unavailable components had inertial properties similar to components being replaced—that is, the weight, the center of gravity, and the moments of inertia of the mockups were identical to those of the components.

Appendix A lists the hardware assemblies that were dynamically qualified at type-approval levels on the *Mariner* Venus 67 STM. There were three classes of units tested: (1) new designs, (2) modifications of *Mariner* Mars 1964 designs, and (3) verifications of existing designs qualified during the *Mariner* Mars 1964 program.

The adapter[2] was structurally complete; it incorporated the spacecraft ejection springs and other spacecraft-adapter interface components, together with their supporting structure.

B. Implementation

1. Test setup. The structural test model was mounted on the *Mariner* Venus 67/*Agena D* adapter which, in turn, was mounted to the appropriate shake fixture for torsional excitation parallel to the roll axis and in three other lateral directions. Test setups for torsional and axial excitation are illustrated by Figs. 1 and 2. Figure 3 shows a typical lateral test setup. Forced vibration excitation was introduced to the STM by means of electromechanical shakers. Torsional excitation was provided by three 1200-lb shakers, placed 120 deg apart, as illustrated in Fig. 1. Excitation for lateral and axial testing was accomplished with one 30,000-lb shaker, as illustrated in Figs. 2 and 3.

The STM was tested in two major configurations: (1) design ultimate-load tests were performed only on a test structure containing four prototype solar panels; (2) solar-panel qualification testing was performed on the test structure containing three prototype panels and one flight-type solar-cell panel. Tests to obtain the dynamic-response characteristics of the post-injection propulsion system for fuel/pressure configurations, as listed in Table 1, were performed on the test structure containing all prototype solar panels.

The sequence of testing, the frequency range employed, the load levels used, and other pertinent data are shown in Table 1. The sequence of testing was established at the time of test because the scheduling was contingent on the delivery date of the celled solar panel and on the time required to interchange panels vs the time required to interchange test axes of the spacecraft.

All vibration testing of the STM was conducted at the JPL Environmental Test Laboratory, in accordance with Environmental and Dynamic Testing Section Procedures.[3]

2. Vibration control. Vibration control of the test structure was accomplished through the use of six piezoelectric-type accelerometers mounted on the test fixture near the fixture/adapter interface (see Figs. 1, 2, and 3). The control circuit for sinusoidal excitation used for the STM test was capable of controlling the acceleration input to the test structure from the six control points, and automatically switching to a constant-value force control if the maximum shaker output force exceeded a pre-set value. Peak acceleration control was maintained by the vibration control system by continuously monitoring the output of each of the six transducers and controlling the total acceleration input to the test structure on the one accelerometer that had the highest output signal. Examples of actual control acceleration are given in Figs. 4 and 5 for spacecraft x and z axes excitation. This control technique limits the maximum acceleration at each of the six control points to the desired level. Functional block diagrams of the control circuit for sinusoidal vibration are given in Figs. 6 and 7. For torsional excitation, the shaker armature current was connected in series to the three shakers. Since the vector force of each shaker had the same phase, the three shakers could drive one torsional test fixture.

[2] Manufactured by Lockheed Missiles and Space Co., Sunnyvale, California; LMSC drawing No. 1364839.

[3] "Vibration System Operations, *Mariner* Venus Structural Test Model (STM) Structural and Environmental Qualification Test," JPL Proc TP500345, Jet Propulsion Laboratory, Pasadena, Calif., October 20, 1966; "Vibration System Operations, *Mariner* Venus 67 Structural Test Model (STM) System Level Solar Panel Qualification Tests," JPL Proc TP500350, October 20, 1966; and "Vibration System Operations, *Mariner* Venus 67 Structural Test Model (STM) Follow-up Structural and Environmental Vibration Qualification Test," JPL Proc TP500400, November 7, 1966. (Specifications are available to qualified requesters.)

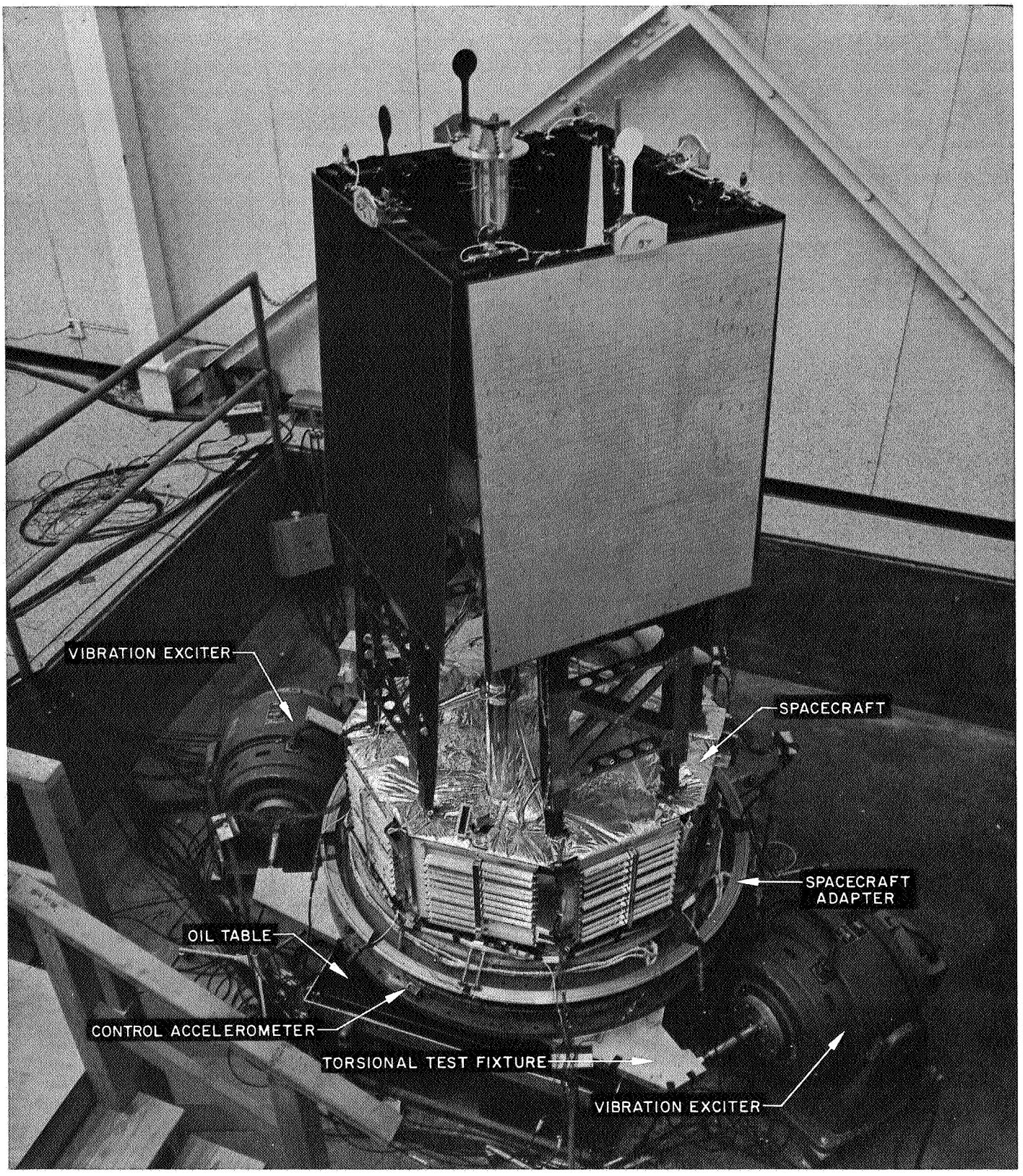

Fig. 1. Torsional test setup

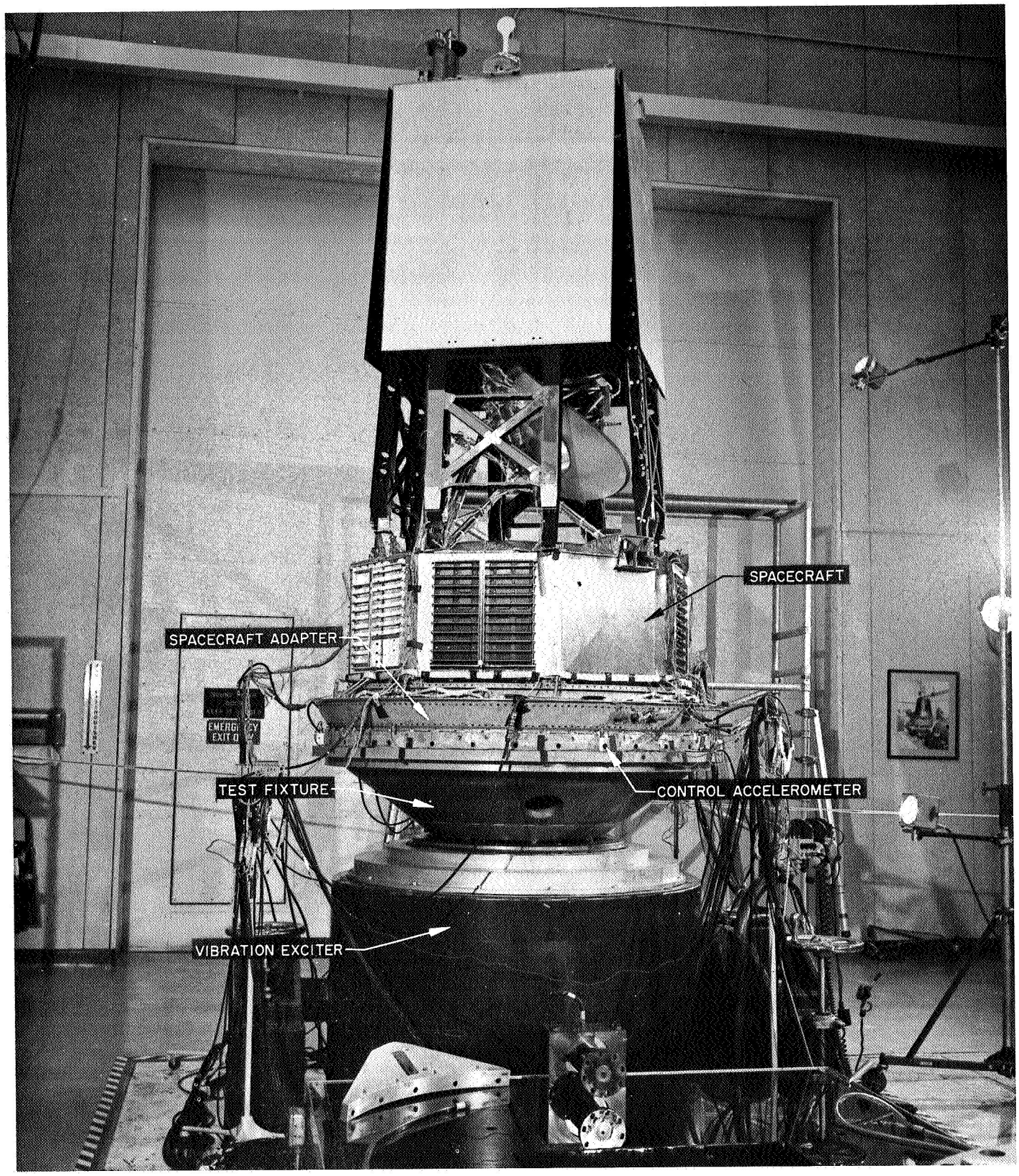

Fig. 2. Axial test setup

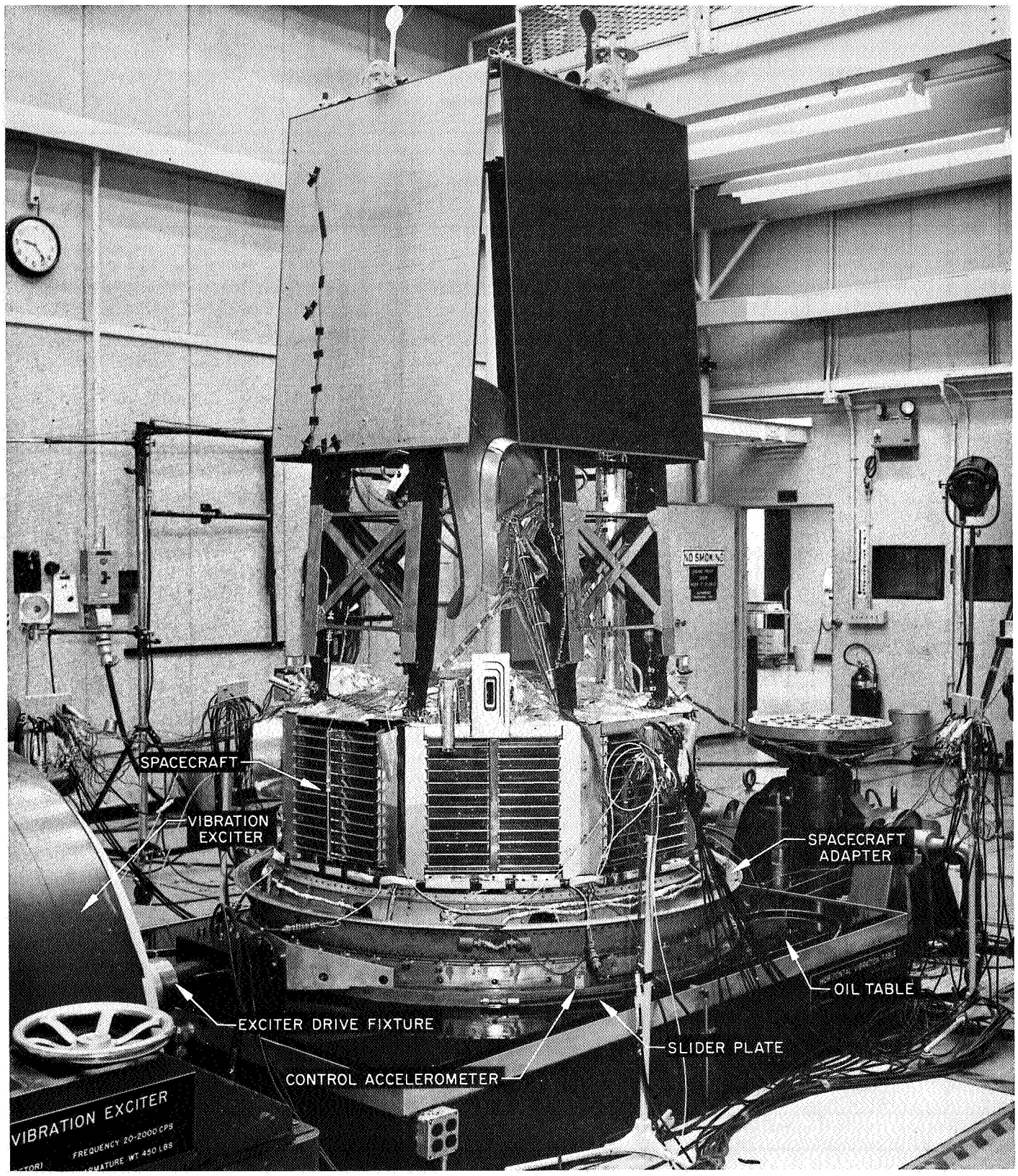

Fig. 3. Lateral test setup

Table 1. Summary of *Mariner* Venus 67 STM test runs

a. *First test series*

Run No.	Axis of excitation	Frequency range, Hz	Control-acceleration levels, g rms	Sweep time, min	Test load category	Date of run, 1966	Remarks[a]
53	Torsional	20–150	6.06 rad/s^2	3.0	Devel.	7/25	Bad dampers, system checkout
54A	Torsional	69, pulse	48.4 rad/s^2	0.14 s	Devel.	7/26	Bad dampers, system checkout
53R	Torsional	20–150	6.06 rad/s^2	3.0	Devel.	7/28	Damper Mod. I system checkout
56A	Torsional	20–150	9.6 rad/s^2	3.0	Limit	7/28	Damper & system equalization and qualification
56U	Torsional	20–150	12.86 rad/s^2	3.0	Ultimate	7/28	System satisfactory
56D	Torsional	150–20	12.86 rad/s^2	3.0	Ultimate	7/28	System satisfactory
54	Torsional	69, pulse	205 rad/s^2	0.14 s	Ultimate	7/28	System satisfactory
55A	Torsional	20–100, pulse			Devel.	7/28	Inst. noise level high
55	Torsional	20–100, pulse			Ultimate	7/28	Inst. noise level high
55R	Torsional	20–100, pulse			Ultimate	7/29	Noise eliminated, system OK
58	x	5–200	0.5	5.3	Devel.	8/2	System verification
60U	x	5–72	1.0	3.8	Ultimate	8/2	Dampers bottomed & run stop
60UR	x	55–200	1.0	1.9	Ultimate	8/2	No damage, continued run
60D	x	200–5	1.0	5.3	Ultimate	8/2	Dampers bottom at 8 Hz
58R	x	5–200	0.5	5.3	Devel.	8/4	Damper Mod. II system OK
59U	x	5–200	0.75	5.3	Limit	8/4	System satisfactory
59D	x	200–5	0.75	5.3	Limit	8/4	System satisfactory
63	x–y, bay II	5–200	0.5	5.3	Devel.	8/4	System verification
64AU	x–y, bay II	5–200	0.75	5.3	Limit	8/4	System satisfactory
64AD	x–y, bay II	200–5	0.75	5.3	Limit	8/4	Slight bottoming at 8 Hz
64U	x–y, bay II	5–200	1.0	5.3	Ultimate	8/4	Bottoming 6 Hz, no damage
64D	x–y, bay II	200–5	1.0	5.3	Ultimate	8/4	Bottoming 10 Hz, no damage
61	x–y, bay VIII	5–200	0.5	5.3	Devel.	8/4	System verification
62AU	x–y, bay VIII	5–200	0.75	5.3	Limit	8/4	System satisfactory
62AD	x–y, bay VIII	200–5	0.75	5.3	Limit	8/4	System satisfactory
62U	x–y, bay VIII	5–200	1.0	5.3	Ultimate	8/4	Bottoming 8 Hz, no damage
62D	x–y, bay VIII	200–5	1.0	5.3	Ultimate	8/4	Bottoming 8 Hz, no damage
65	z	5–200	1.0	5.3	Devel.	8/8	System verification
66AU	z	5–200	1.5	5.3	Limit	8/8	System satisfactory
66AD	z	200–5	1.5	5.3	Limit	8/8	System satisfactory
66U	z	5–200	2.0	5.3	Ultimate	8/8	System satisfactory
66D	z	200–5	2.0	5.3	Ultimate	8/8	System satisfactory
71	z	5–200	1.0	5.3	Devel.	8/11	Celled panel, PIPS Δf
72U	z	5–200	1.5	5.3	Limit	8/11	System satisfactory
72D	z	200–5	1.5	5.3	Limit	8/11	System satisfactory
73	z	550–2000	18.1	3.0	Limit	8/11	System OK; lost 2 accelerations
74	x	5–200	0.5	5.3	Devel.	8/12	System verification
75U	x	5–200	0.75	5.3	Limit	8/12	System satisfactory
75D	x	200–5	0.75	5.3	Limit	8/12	System satisfactory
76F	x	550–2000	6.1	3.0	Devel.	8/12	4 low-level runs for equalization
76	x	550–2000	18.1	3.0	Limit	8/12	Erratic low *f* motion

[a] *System* refers to the entire test implementation and test-specimen response parameters.

Table 1a (contd)

Run No.	Axis of excitation	Frequency range, Hz	Control-acceleration levels, g rms	Sweep time, min	Test load category	Date of run, 1966	Remarks[a]
80	x–y, bay II	5–200	0.5	5.3	Devel.	8/13	System verification
81U	x–y, bay II	5–200	0.75	5.3	Limit	8/13	Rattling in monoballs
81D	x–y, bay II	200–5	0.75	5.3	Limit	8/13	Same, system satisfactory
82	x–y, bay II	550–2000	18.1	3.0	Limit	8/13	Slight low f shift
79	x–y, bay VIII	550–2000	18.1	45 s	Limit	8/13	Transfer function information
67	z	5–200	1.0	5.3	Devel.	8/16	PIPS 300 psi, run OK
68	z	5–200	1.0	5.3	Devel.	8/16	PIPS 400 psi, run OK
69	z	5–200	1.0	5.3	Devel.	8/16	PIPS 0 psi, run OK
70	z	5–200	1.0	5.3	Devel.	8/16	PIPA empty, run OK
b. Follow-up test runs							
83	x	200–20–200	0.5	3.6	Flight	11/7	Preflight system check
84U	x	5–200	0.75	5.3	Limit	11/7	System satisfactory
84D	x	200–5	0.75	5.3	Limit	11/7	System satisfactory
86	x	550–2000	10.7	1.0	Flight	11/7	Preflight system check
87	x	550–2000	18.1	3.0	Limit	11/7	System satisfactory
88	x–y, bay II	200–20–200	0.5	3.6	Flight	11/9	Panels noisy; retorqued
89U	x–y, bay II	5–200	0.75	5.3	Limit	11/9	System satisfactory
89D	x–y, bay II	200–5	0.75	5.3	Limit	11/9	System satisfactory
91	x–y, bay II	550–2000	10.7	1.0	Flight	11/9	Preflight system check
92	x–y, bay II	550–2000	18.1	3.0	Limit	11/9	System satisfactory
93	z	200–5–200	1.0	3.6	Flight	11/11	SS1 & SS4 high noise level
98	z	20–200	1.0	3.6	Devel.	11/11	1.0 octave/min sweep rate
99	z	20–200	1.0	0.9	Devel.	11/11	4.0 octaves/min sweep rate
100	z	20–200	1.0	0.28	Devel.	11/11	11.48 octaves/min sweep rate
101	z	20–200	1.0	0.23	Devel.	11/11	14.57 octaves/min sweep rate
94U	z	5–200	1.5	5.3	Limit	11/11	System satisfactory
94D	z	200–5	1.5	5.3	Limit	11/11	System satisfactory
96	z	550–2000	10.7	1.0	Flight	11/11	Preflight system check
97	z	550–2000	18.1	3.0	Limit	11/11	HG-2, -3, -4 lost; system OK

[a] *System* refers to the entire test implementation and test-specimen response parameters.

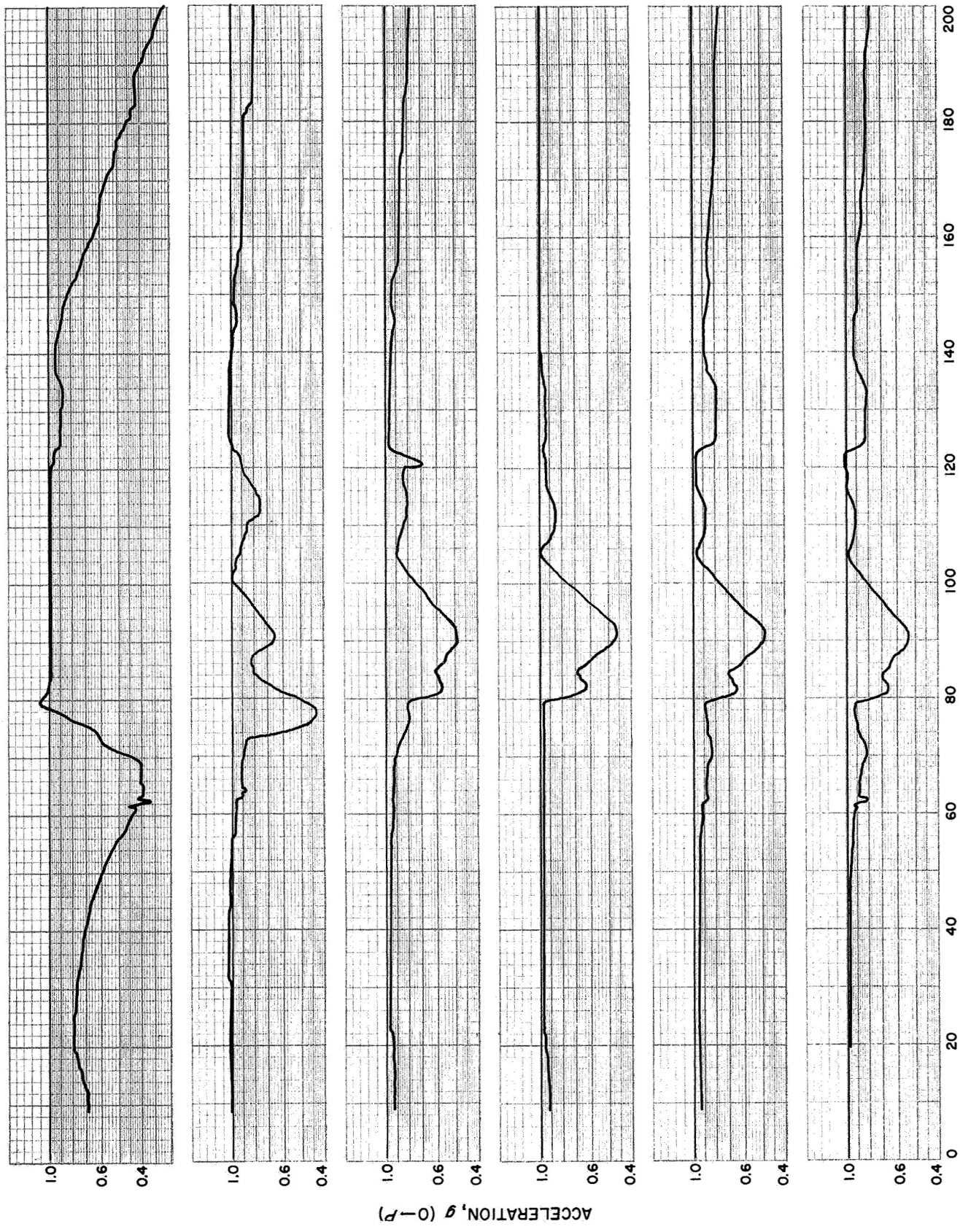

Fig. 4. Control accelerometers 1 through 6 for spacecraft x-axis excitation, run 84U

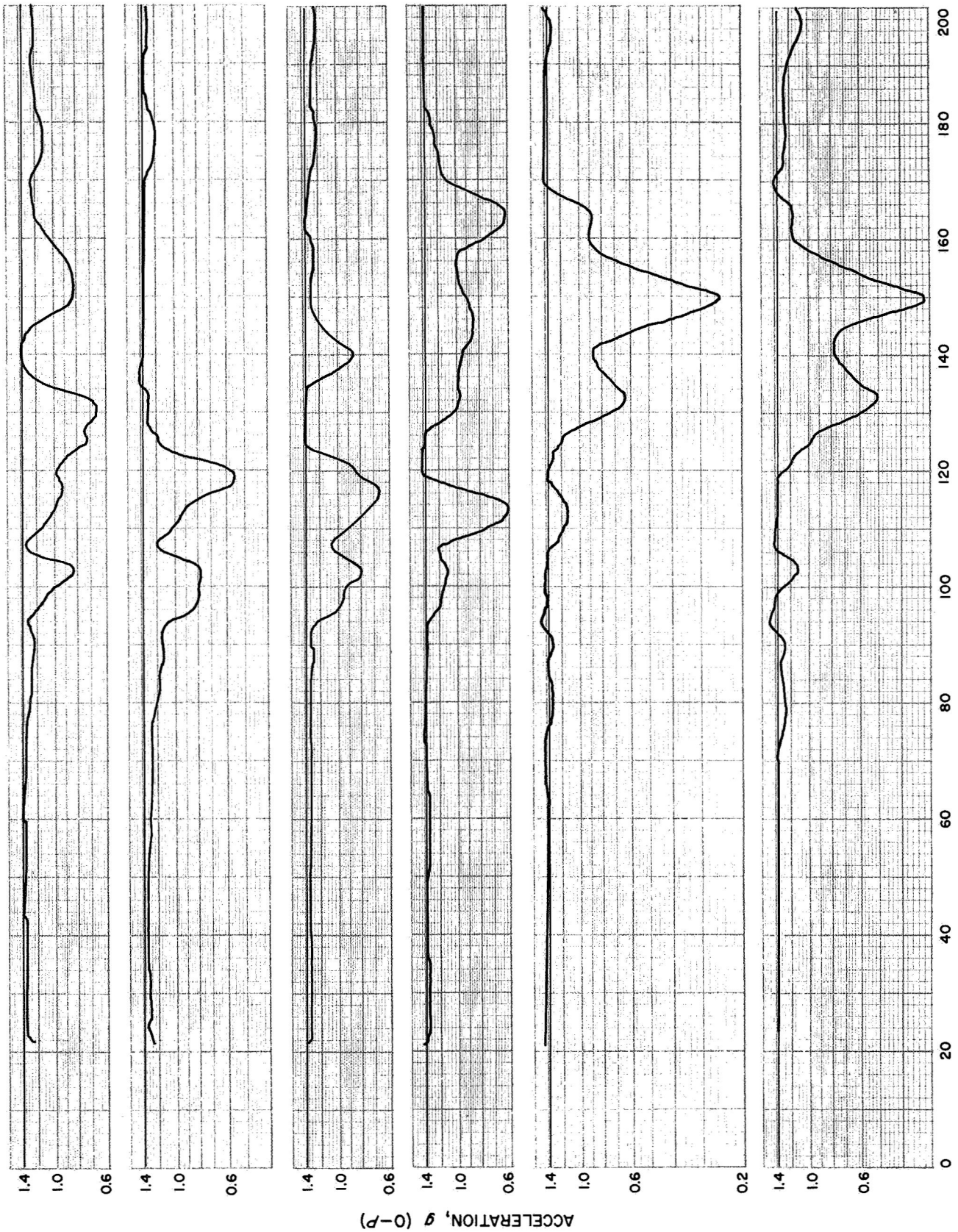

Fig. 5. Control accelerometers 1 through 6 for spacecraft z-axis excitation, run 93

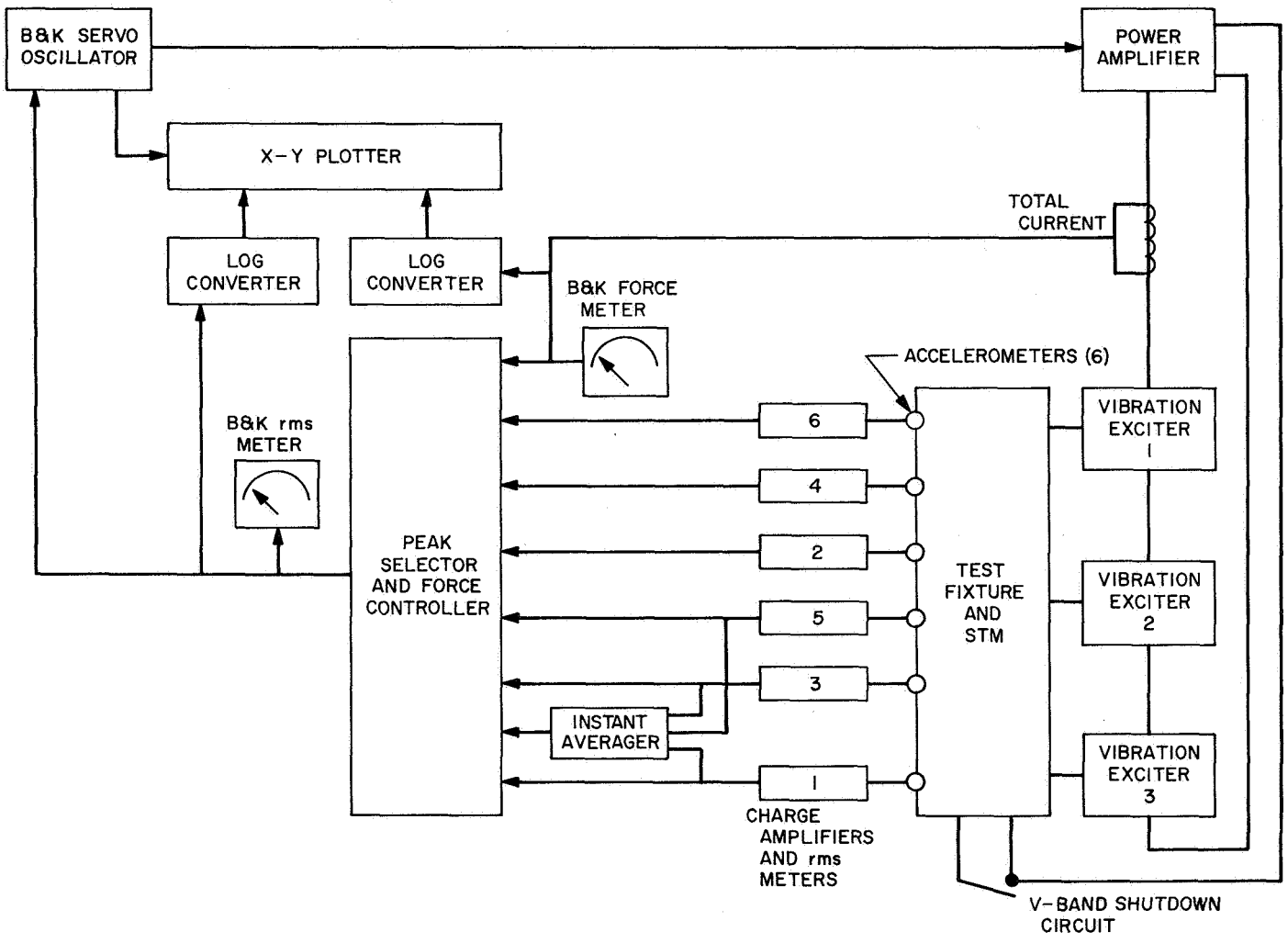

Fig. 6. *Torsional sine sweep test, functional block diagram*

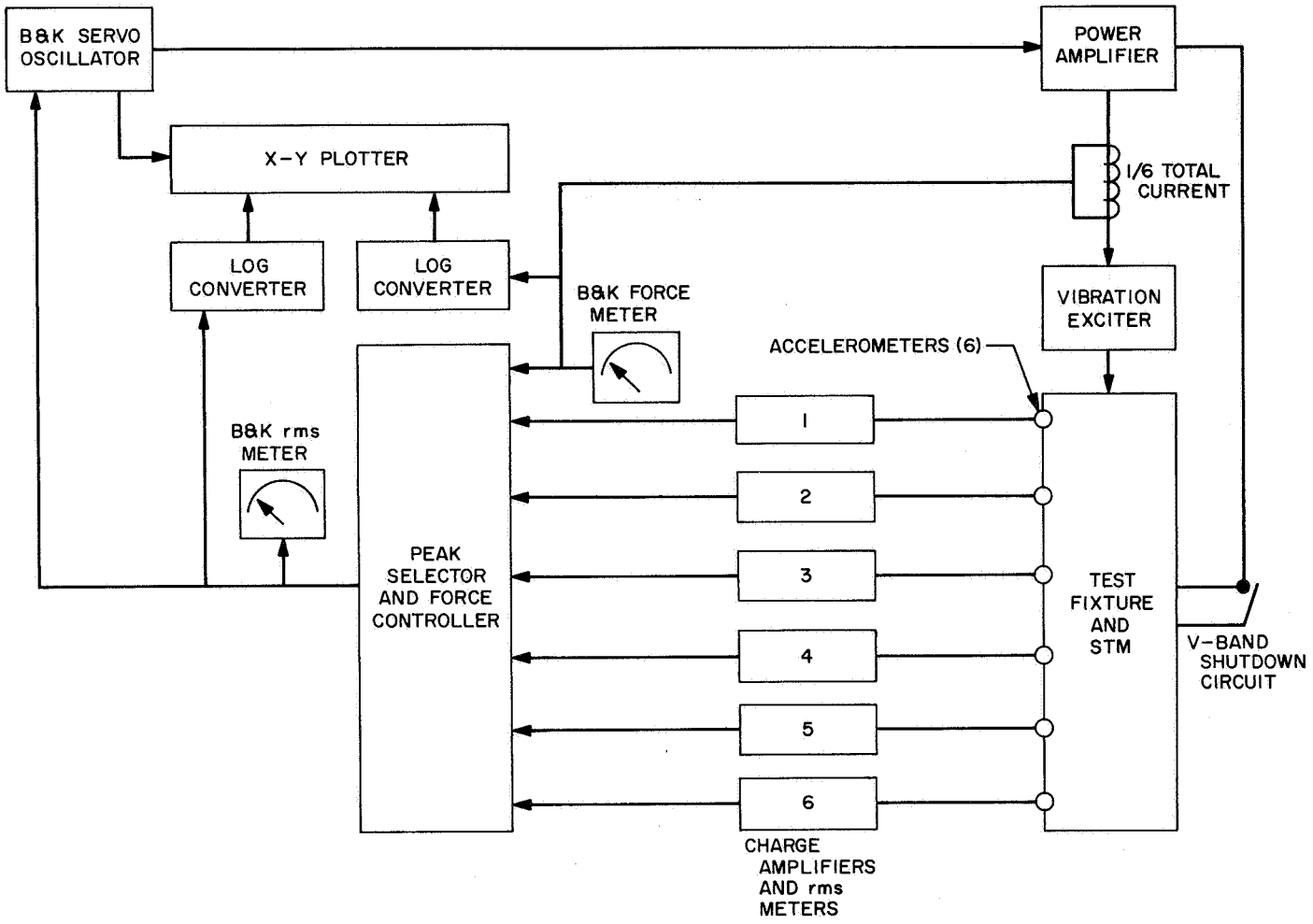

Fig. 7. Sine test control circuit, functional block diagram

Two different implementation techniques were used for the vibration control of transient-type torsional acceleration. The first type required no equalization of the signal from the electromagnetic tape containing the desired acceleration spectrum. Therefore, it played directly through the power amplifier, as shown in Fig. 8. (Refer to Appendix C for details of the pulses.) The second method utilized standard peak and notch filters to condition the signal from the electromagnetic tape before entering the power amplifier. (Refer to Fig. 9 for functional block diagram.) An evaluation of the two methods is given in Section III-E.

An independent safety control circuit to protect the spacecraft in case of V-band failure was used. In case of V-band failure, this circuit would reduce the amplitude of forced vibration to zero, with transients not deleterious to the test structure (Figs. 6 through 9).

3. Instrumentation. Control- and response-accelerations of the test structure were measured with piezoelectric-type accelerometers. Wherever possible, response accelerometers were attached to the test structure with screw attachments. For more delicate hardware—such as the high-gain antenna, solar panels, and some science instruments—bonded attachments were acceptable. Screw attachments were mandatory for all control-accelerometers.

The total accelerometer system frequency vs amplitude response was within $\pm 5\%$ from 5 to 2000 Hz. The total accelerometer system amplitude linearity was within $\pm 5\%$ deviation from the best representative straight line between zero and the full-scale range of the measurement. The total noise from the accelerometer system, with the transducers mounted on the STM, was less than 0.2 g rms.

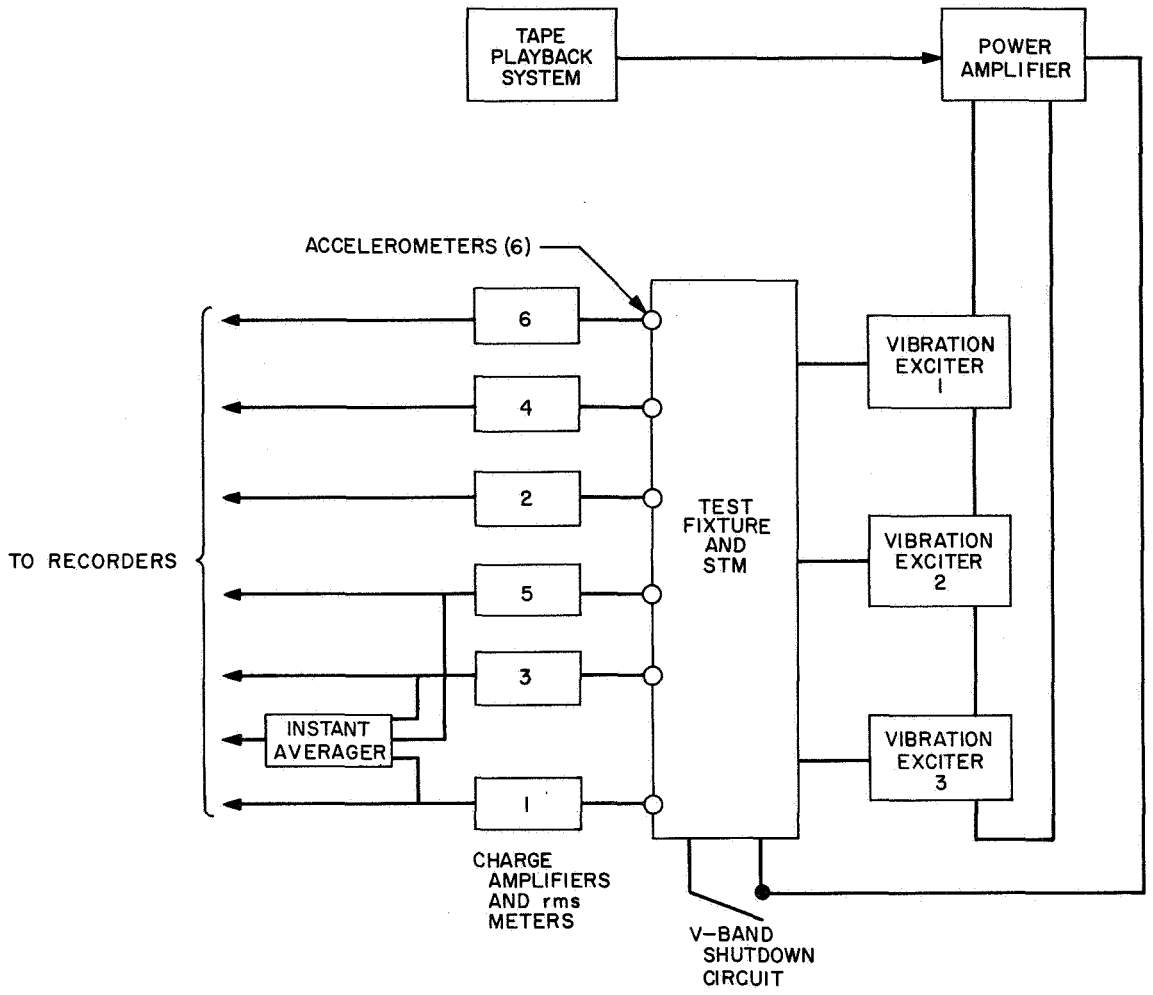

Fig. 8. Torsional pulse tests without signal equalization, functional block diagram

Dynamic strain information was obtained with strain gages. Strain gages were mounted on the clevis of two solar-panel boost dampers, wired and calibrated so that their output signal was proportional to the dynamic load, in pounds, across each solar-panel tip damper. This was feasible since the local resonance of the strain-gaged dampers was well above the frequency of response of the solar-panel structure.

The output signals of all control- and response-transducers were recorded on electromagnetic tape to provide for flexibility of data reduction. Twelve channels of selected rms acceleration response were recorded on a direct-write oscillograph for each test run as a plot of dc amplitude vs frequency for sine excitation tests. The oscillograph was run at such a slow speed that the plot of dc acceleration envelope vs sweep frequency for one complete test run was displayed on a 12- by 24-in. recorder for quick-look data analysis.

The load links in the spacecraft V-band assembly were strain gaged and calibrated to read load in pounds. Tension in the V-band was monitored before and after each forced vibration test on a strip-chart potentiometer recorder for a permanent record.

Detailed instrumentation run sheets containing information on types of transducers used, orientation and locations of transducer mountings, and electromagnetic tape channel identification are given in Appendix B. Each transducer mounting has been documented photographically for future reference.[4]

C. Test Loads

Structural qualification vibration loads as defined in JPL specifications (see footnote 1) were applied to the

[4] The photographs are with the JPL Applied Mechanics Section records; they are available to qualified requesters.

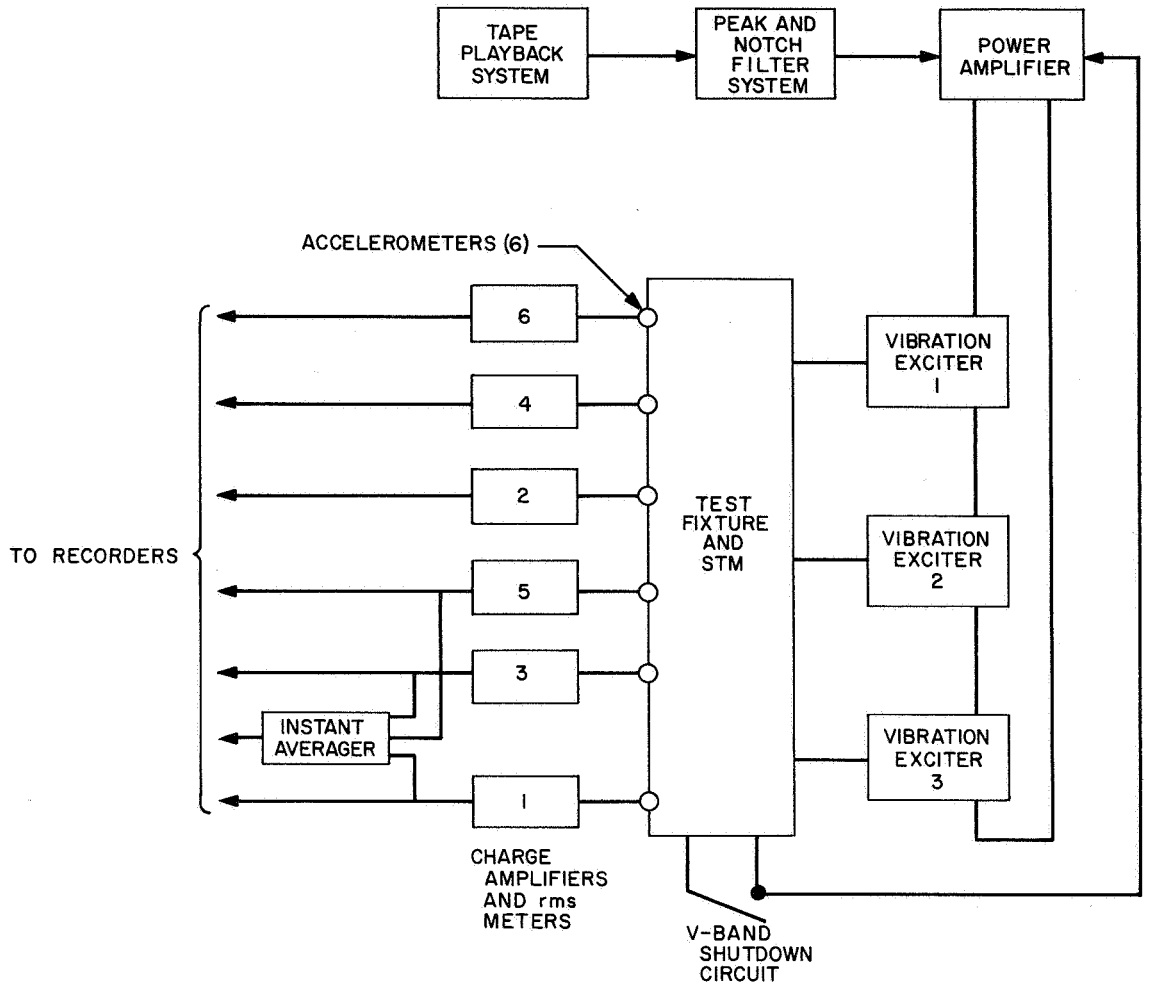

Fig. 9. Torsional pulse test with signal conditioning, functional block diagram

STM of the *Mariner* Venus 67 vehicle. The multifrequency torsional transient qualification load requirements were derived from an analysis that is presented in detail in Appendix C.

Low-level excitation was introduced to the test structure for each run listed in Table 1 prior to full-level testing. From the low-level tests the predicted response of pertinent structural elements was evaluated from direct-write oscillograph plots. This procedure also allowed system verification before the introduction of qualification loads.

III. Discussion of Test Results

The actual total test time for which the STM underwent the forced-vibration excitation necessary to satisfy all the objectives of the test program was 270 min.

During the testing program, two modifications were made on the solar-panel tip dampers. The initial damper-test hardware was found to be undesirable for qualification testing; improved damping characteristics were obtained by changing the size of the sealing O-rings and changing the viscosity of the damping fluid. Qualification and design ultimate-load-level testing was performed, without failure, with the modified hardware for torsional and x-axis excitation. During x-axis excitation at design ultimate-load level (run 60U, Table 1), large dynamic excursions of the dampers at 8 Hz resulted in boundary contact between the end of the damper piston and the damper housing. Even though the dynamic loads associated with this shock-type acceleration were not deleterious to the structure, the dampers were removed from the test structure and mechanically adjusted to provide for larger dynamic displacements. The boundary contact, which occurred only at design ultimate-load level in

lateral axes of excitation, was greatly reduced during the remainder of the test.

Two other pieces of hardware were repaired during the testing program: The attitude-control-jet sunshade support brackets in bays I and VII experienced spot-weld failure, and one lexan tube fitting on the high-gain antenna-feed support structure developed a crack during design ultimate-load-level testing in the z axis (run 66U, Table 1). After completion of the STM test, and prior to use of the STM as a test fixture for the solar-panel system-level qualification test, the fitting was preloaded in the hoop direction by using a wire wrapping that was potted with epoxy. A small hole was drilled at the apex of the crack to prevent a potential stress concentration. The crack appeared not to propagate during the remainder of the test program. The failure of the tube fitting was of no structural significance, since that particular piece of hardware had previously undergone several complete dynamic-test programs for the *Mariner* Mars 1964 program.

The dynamic-response characteristics of some of the major elements of the spacecraft are different from those of the *Mariner* Mars 1964; the geometric change of these elements has resulted in entirely different dynamic-response characteristics, especially of the solar panels and high-gain antenna support structure, and somewhat of the secondary structure, the PIPS and the omnidirectional antenna. Nonlinear behavior was still exhibited by the solar-panel boost dampers and bladder-fuel sloshing in the PIPS fuel tank.

A. Spacecraft V-Band

The variation of V-band tension resulting from dynamic forces imported to the test structure was obtained from recordings made before and after each test run. Analysis of these data indicates no definite trend of V-band tension variation with respect to test parameters, but it rather strongly indicates a normal distribution of tensions for the composite of all test data. For this reason, it was

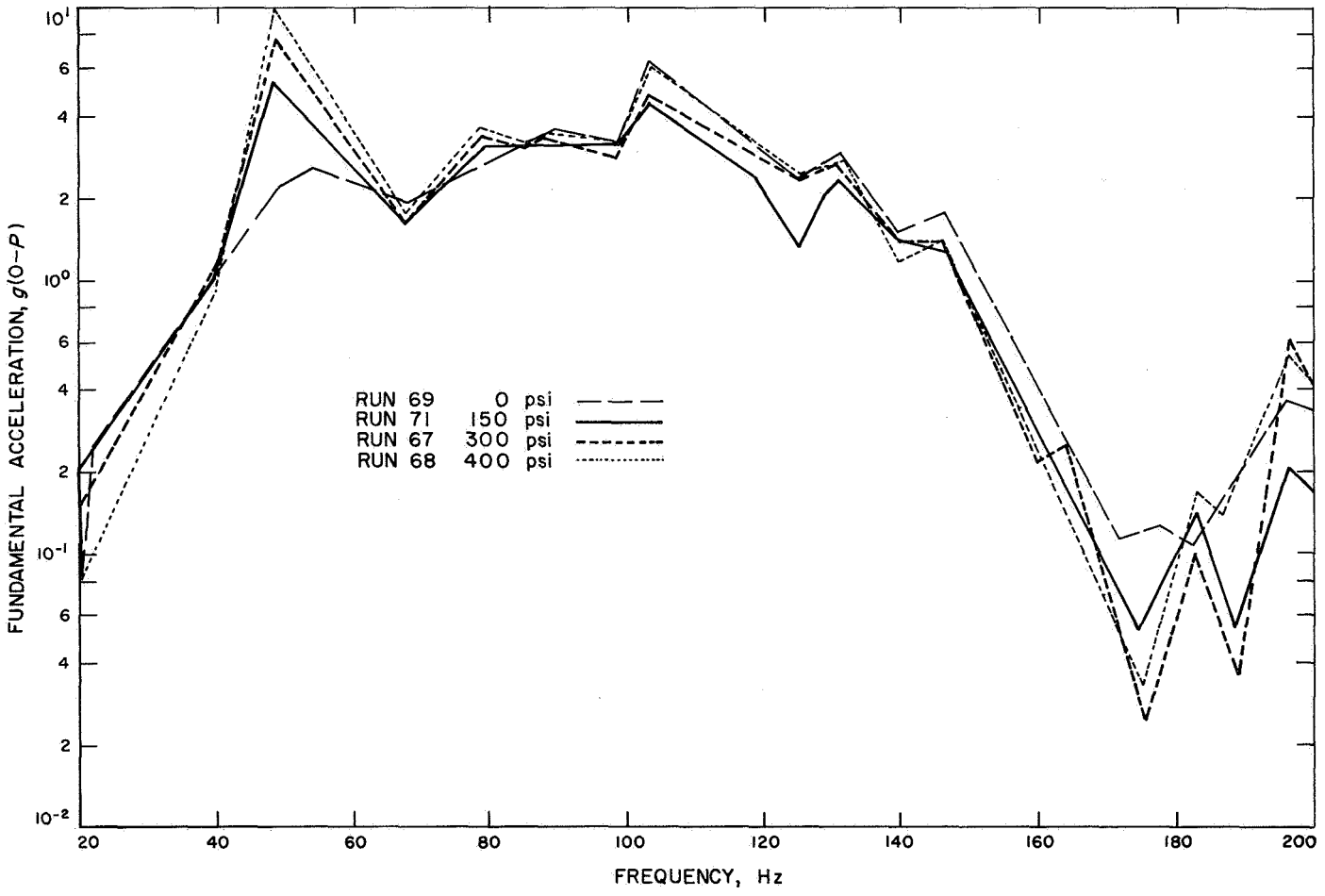

Fig. 10. Effect of fuel tank pressurization on response of PIPS

decided to treat the test data statistically, assuming a normal distribution.

The eight values of V-band tension, recorded before and after each test run, were averaged. These mean values, based on 84 sets of recordings, were used to obtain the sampling distribution of means of each sample. The 2500-lb mean value of V-band tension was obtained from the mean value of the sampling distribution. An estimate of the variance of tension values was obtained from the dispersion of the sampling distribution of mean values. One standard deviation of V-band tension for any particular spacecraft bay was 27.6 lb.

Nominal flight V-band tension is 2500 lb, with an allowable variation of ±25 lb on the initial tension and ±50 lb variation for flight. Variations seen during the test were more than adequate to maintain the necessary preload between the spacecraft and its adapter during the boost phase of flight.

B. Post-Injection Propulsion System

The dynamic response of the PIPS for excitation applied to the base of the STM is entirely dependent on the pressure in its bladdered fuel tank. This highly nonlinear behavior is caused by pressure-dependent fluid sloshing in the fuel tank. Figure 1 illustrates the acceleration response of the PIPS support frame at the point of attachment of the thrust plate for different fuel-tank pressures as obtained from the STM for 1 *g* rms input along the *z* axis of the spacecraft—the most critical spacecraft axis of excitation for the PIPS. Modes of structural response at 49, 104, and 197 Hz for pressure variations are shown in Fig. 10. The response mode at 49 Hz is most significant; the pressure-dependent amplification factor is the greatest, with generalized mass being largest for this mode, and thereby, the greatest reaction loads are induced to the bus structure. The effect of the PIPS response on other spacecraft elements is shown in Fig. 11. This figure shows the relationship between fuel-tank pressure and the response of other spacecraft elements at 49 Hz for 1 *g* rms input to the STM along the *z* axis. Since the entire test structure is affected by the pressure-dependent responses of the PIPS, 150 psi in the fuel tank was used as a compromise between realism and safety for all tests except one special test in the *z* axis. This special test was run to obtain response data for fuel-tank pressures from zero to full-flight pressure.

Modes of structural response of the PIPS at 49 and 104 Hz are characterized by maximum acceleration

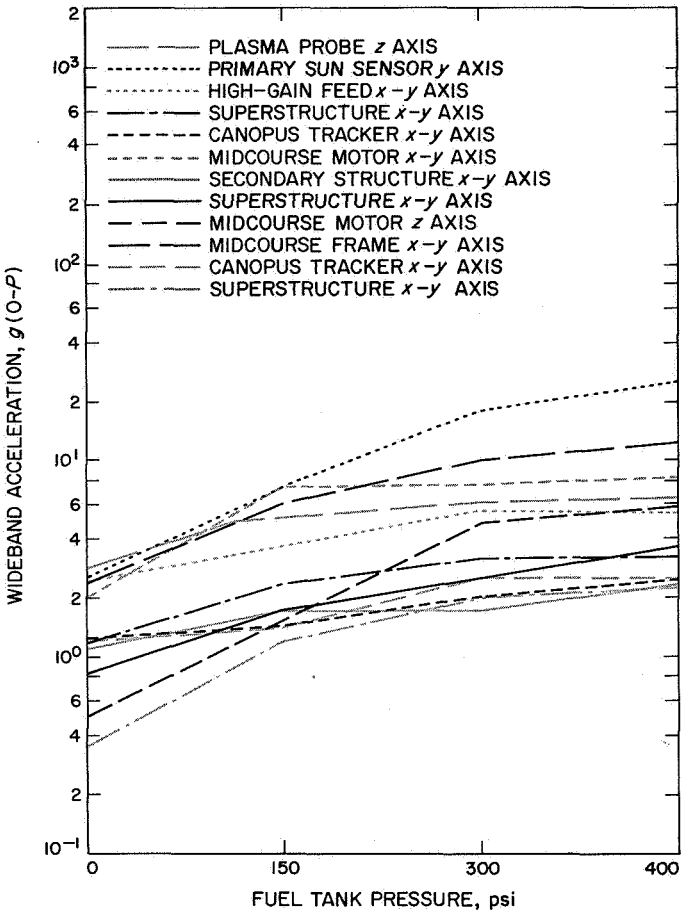

Fig. 11. Effect of PIPS response on other spacecraft elements for several fuel tank conditions

response near the center of gravity of the fuel tank, brought about by elastic deformation of the fuel tank, fuel-tank support structure, and the PIPS support frame. The first mode is a rocking-type mode of the thrust plate about an axis perpendicular to the thrust axis of the motor. The second mode is a combination of translation and rotation of the fuel tank about a nonsymmetric axis almost parallel to the thrust plate. Correlation of analysis and test for the frequency of the first two response modes was very good.

C. High-Gain Antenna

The dynamic response of the *Mariner* Venus 67 high-gain antenna and superstructure was found to be somewhat different from the dynamic response of the corresponding components of the *Mariner* Mars 1964. Figures 12 and 13 present pertinent response data at the tip of the antenna dish vs input acceleration at the base of the spacecraft for both the *Mariner* Venus 67 and the *Mariner* Mars 1964 spacecraft system-level test. The

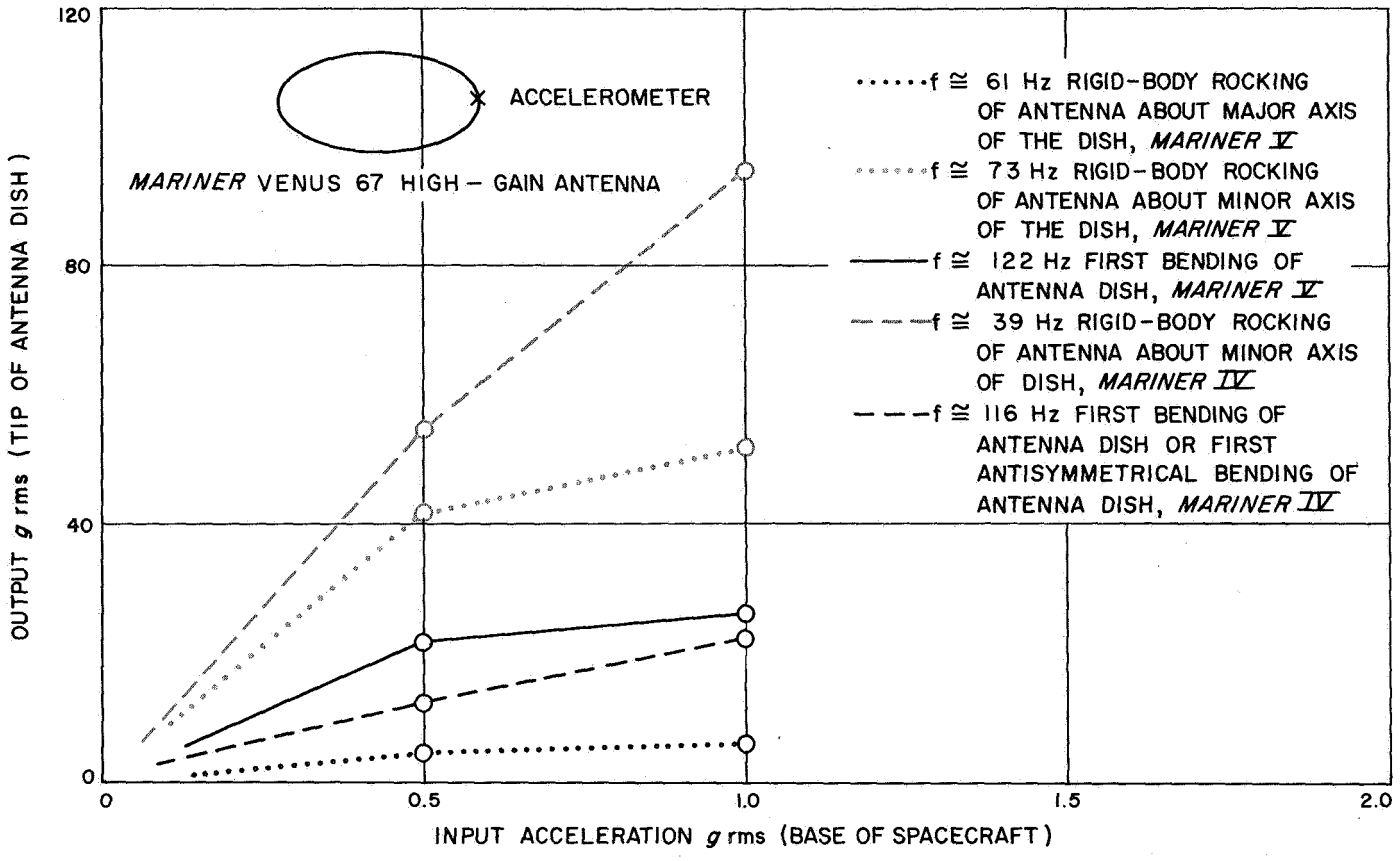

Fig. 12. High-gain antenna dish response to spacecraft x–y axis excitation

different antenna-dish responses of the *Mariner* Venus 67 and the *Mariner* Mars 1964 result from the different superstructure used for the *Mariner* Venus 67 antenna. The first two natural modes of vibration of the *Mariner* Venus 67 antenna are functions of the antenna-support-structure geometry. The first mode is a rigid-body rocking motion about the major axis of the antenna, and the second mode is a rigid-body rocking motion about the minor axis of the antenna. The three-point support connection of the *Mariner* Venus 67 antenna to its superstructure allows this type of rigid-body motion about both the major and minor axes of the antenna dish. The *Mariner* Mars 1964 antenna was constrained from rotating about its major axis by the five-point support connection of the antenna to its support structure. The frequency of the first natural mode of the *Mariner* Venus 67 antenna is substantially higher than that of the *Mariner* Mars 1964 antenna because of this much stiffer support structure.

The elastic responses of the *Mariner* Venus 67 and the *Mariner* Mars 1964 antennas were similar, as could be expected, since the elastic response of the antenna dish is essentially independent of the support-structure geometry. In Fig. 13, however, it is seen that for excitation in the spacecraft z axis there is a substantial increase in the response at the tip of the *Mariner* Venus 67 antenna dish for the second elastic bending mode (132 Hz) of the antenna dish over the corresponding mode of the *Mariner* Mars 1964 antenna dish. Analysis and test indicate that there is dynamic coupling between the *Mariner* Venus 67 second elastic bending mode of the antenna dish and a twisting-type mode of the superstructure at 132 Hz, resulting in the higher response output at the tip of the antenna dish. This high-acceleration output is not detrimental to the antenna.

The STM test was found to be satisfactory for testing the adequacy of the *Mariner* Venus 67 high-gain antenna and superstructure to withstand qualification vibrational loading. Theoretical analysis was found to be in good agreement with the STM response analysis for the first four natural modes of the antenna and superstructure.

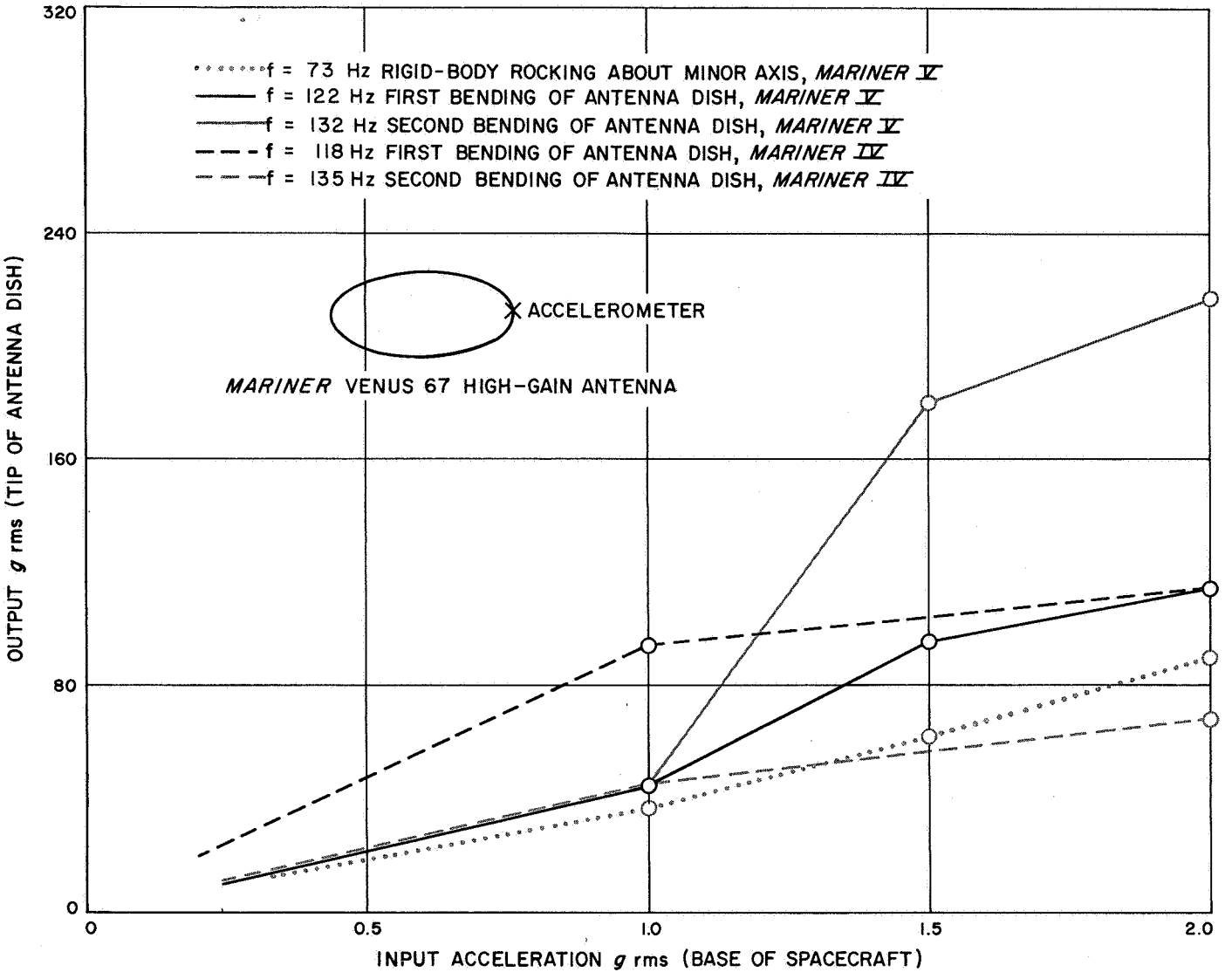

Fig. 13. High-gain antenna dish response to spacecraft x-axis excitation

D. Solar Panels

Comparison between test and analysis is given for solar panel 1 in Fig. 14. In each case, the input to the solar-panel test structure is a sinusoidal, base acceleration along the spacecraft x axis with a nominal amplitude of 1.06 g zero-to-peak, type-approval level. Because of the nonrigid test fixture, only one input monitoring accelerometer at a time could be at this acceleration level. The effect of the nonrigid test fixture on spacecraft flexibility is not included in the analysis; neither is the part-to-part variation of hardware components, but the natural frequencies and damping coefficients of all panels in the analysis have been adjusted to those of the type-approval panel that was modal tested. Frequency variations of hardware observed during flight-acceptance testing were of the order of 10%.

The response accelerations from analysis compared with test data correspond to the acceleration normal to the panel in four locations: near the edge and the top of the substrate of solar panel 1C1; near the edge midway between the top and bottom of solar panel 1C2; near the edge and the bottom of solar panel 1C3; and on the centerline near the bottom of solar panel 1C4 (see Fig. 15).

The test values represent the first fundamental content of the response acceleration for increasing frequency sine

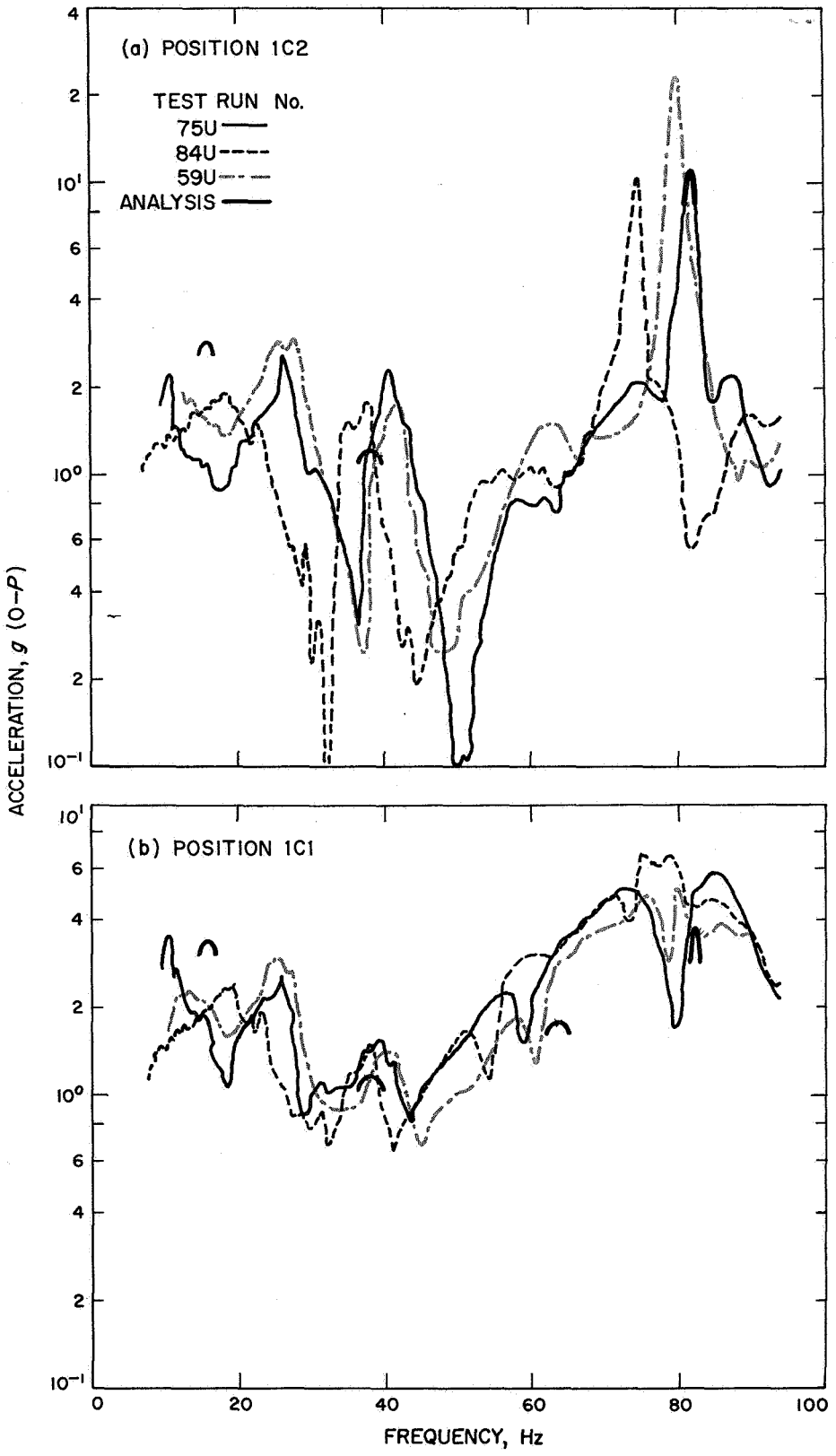

Fig. 14. Comparison of analysis with test data for solar panel corrugation response to spacecraft x-axis excitation

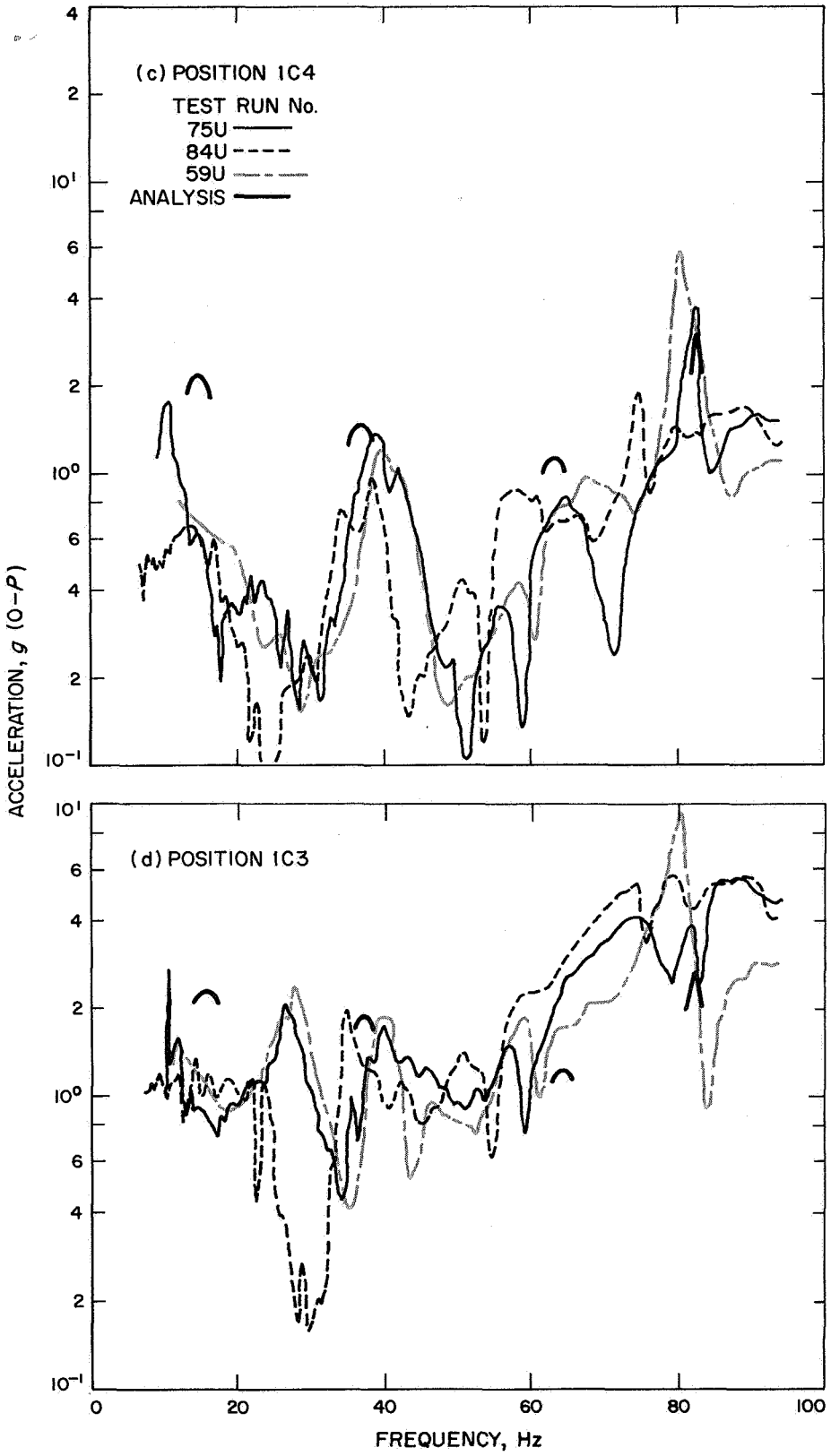
(c) POSITION 1C4
TEST RUN No.
75U
84U
59U
ANALYSIS
(d) POSITION 1C3
ACCELERATION, g (0-P)
FREQUENCY, Hz
0
20
40
60
80
100

Fig. 14 (contd)

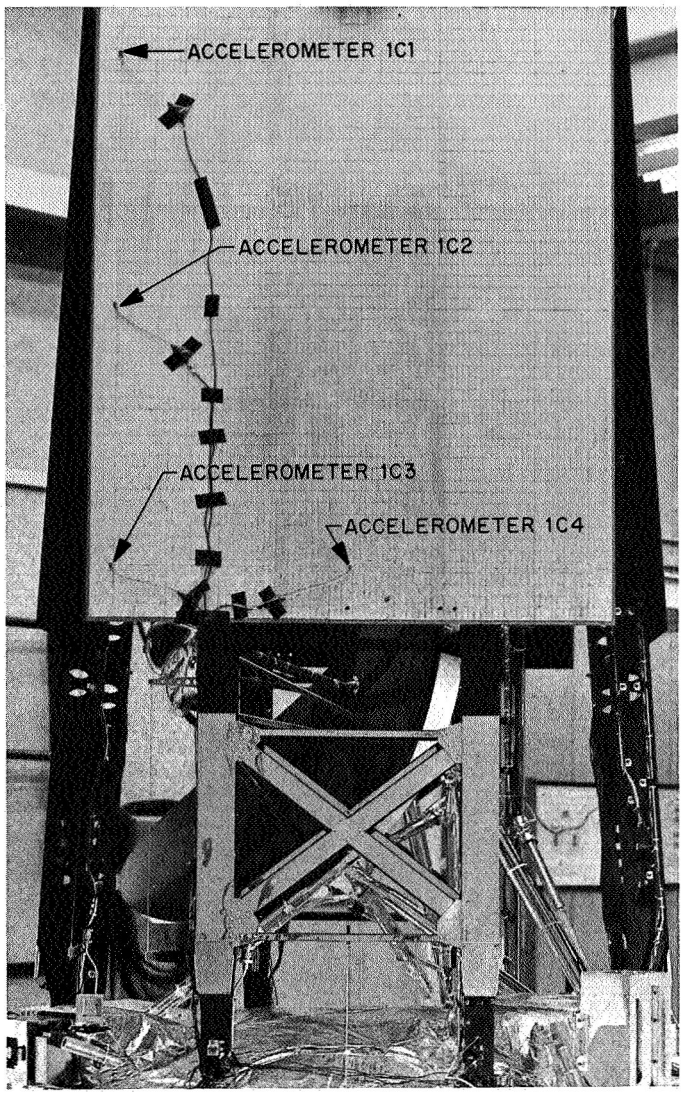

Fig. 15. Location of solar panel response accelerometers

sweeps. The response curve in Fig. 14 is for the first STM test with four dummy panels; for run 59U the test was repeated, with one dummy panel being replaced by the celled panel; run 75U represents the second STM test in which were used modified boost dampers with nominally similar properties of run 84U. Only the peak values of the analytic response are shown, since the calculation method iterates on equivalent linear coefficients for the nonlinear spring dampers, and only the peak values have been evaluated.

Since test values of damping and slightly modified response frequencies based on tests were used in the composite analysis, this refined an analysis can't be performed prior to fabrication of a prototype hardware. On the other hand, to improve the comparison, the as-fabricated properties of the actual components are required.

The response peak near 80 Hz is associated with a well defined substrate mode in which the individual corrugations are supported very near their free node points. Such a mode has a very low ratio of rigid elastic-mass coupling to modal mass, which reduces the predicted response from analysis far below the level of a similarly damped ($C/C_c = 0.002$) one-degree-of-freedom system—for which this ratio is 1.0. For this mode, very small changes in mass distribution can have a drastic effect on the small numbers involved, and large panel-to-panel variation of response can be expected, which will not be damped by the point dampers.

The comparison between test and analysis is within twice the spread of the test data when comparing nearby peaks. The test data exhibits far more peaks than the analysis, indicating that the test part is more complex than the present analytic model.

E. Comparison Between Multifrequency and Modulated-Tone Transient Excitations

The spacecraft was excited at its base with four multiple-frequency pulses derived from the *Ranger* data (see Refs. 1 and 2 and Appendix C) and a 69-Hz modulated-tone pulse. Seventeen locations were chosen as a representative sample of the response of the spacecraft. The objective of this test was to compare the response of the 69-Hz pulse with the response of the multifrequency pulse. Only one of the multifrequency pulses, pulse 3, was investigated.

Comparison of control-acceleration-time histories at the time of the test for the two methods of implementation indicated that the first method used was superior; this fact is also verified by Ref. 1. The voltage equalization performed on the analog computer has more flexibility than a given number of peak and notch filters. Therefore, the acceleration-time histories conformed more closely to that desired when implemented by the preferred method.

The Fourier transform $V_1(f)$ of the pulses $U_1(t)$ has been calculated for all the pulses. Figure 16 shows the time history, the modulus, and the phase angle of the Fourier transform corresponding to pulse 3. Figure 17 shows the time history, the modulus, and the phase angle of the 69-Hz pulse.

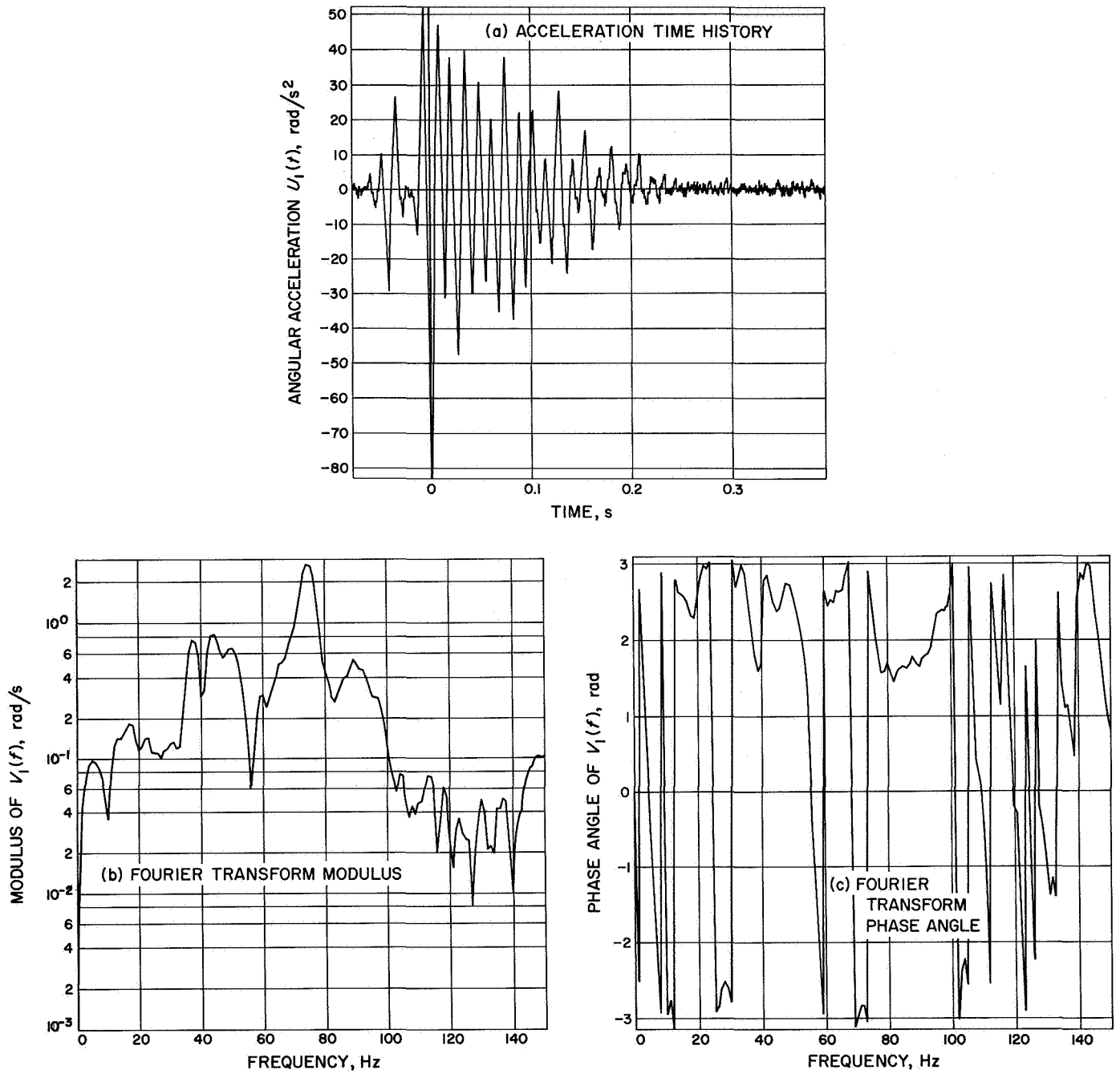

Fig. 16. Test pulse 3 qualification testing

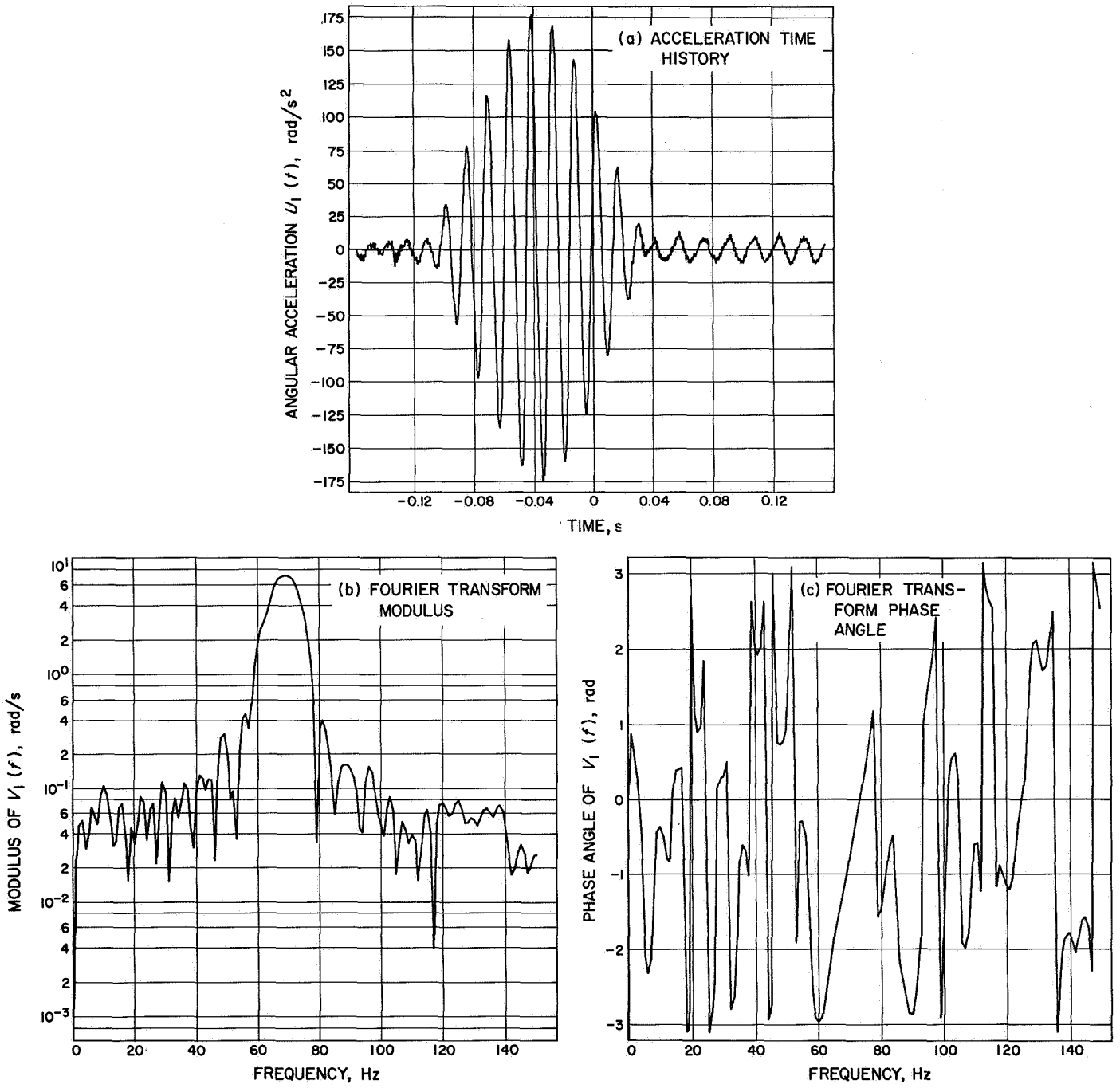

Fig. 17. 69-Hz test pulse qualification testing

Several observations concerning the test data can be made:

(1) The level of the 69-Hz pulse was set much higher than the level for pulse 3 (352 rad/s^2 against 134 rad/s^2 peak-to-peak).

(2) The modulus of the Fourier transform of the 69-Hz pulse exhibits a high peak at 69 Hz with much less amplitude below and above 69 Hz. However, it is worth mentioning that this peak is less sharp than one might expect from a pure tone at constant amplitude, due to the smoothing effect of the modulation which broadens the spectrum.

(3) The modulus of the Fourier transform of the multifrequency pulse 3 derived from *Ranger VIII* data shows a spectrum that is broader than the 69 Hz, with a major peak at 74 Hz and smaller peaks at 37, 44, and 89 Hz. Because of this wider spectrum, it was anticipated that pulse 3 would excite more modes than the 69-Hz pulse and might lead to higher amplitude responses.

The time histories, the moduli, and phase angles of the Fourier transforms of the responses of the spacecraft were determined for the 17 locations mentioned above. Figures 18 and 19 show typical curves for the acceleration-time history, the modulus, and the phase angle of the Fourier transform and represent the response of solar panel 1. The comparison of the peak-to-peak responses for the two types of base accelerations (pulse 3 and 69 Hz) was made in Table 2. Comparison of columns 1 and 2 shows that the 69-Hz pulse gives more amplitude than pulse 3 for all response locations, principally from the much higher level of the 69-Hz pulse, which wipes out the effect of the frequency content of pulse 3. In order to isolate the frequency effect, we raise the level of pulse 3 to the level of the 69-Hz pulse; this means that the levels of column 2 are multiplied by 352/134, or 2.62, to give the levels of column 3. The two base pulses have now the same maximum peak-to-peak levels. It can then be seen, by comparing columns 1 and 3, that 10 out of 17 responses have now a higher level for the excitation with pulse 3 than with the 69-Hz pulse, showing the effect of the wideband spectrum of pulse 3.

Table 2. Comparison of responses

Location	69-Hz pulse, input level 352 rad/s^2	Pulse 3, input level 134 rad/s^2		
	Peak-peak response 69 Hz, g	Peak-peak response pulse 3, g	Peak-peak response for input level same as 69 Hz, g	Deviation of the two pulses, %
Top of bus leg D z-axis	13.0	4.0	10.5	−19
Adapter tangent at foot C	25.7	9.5	24.9	−3
Secondary structure	49.8	16.0	42.0	−16
Antenna support superstructure	30.8	10.45	27.4	−11
High-gain antenna dish	168.0	57.9	152.0	−9
High-gain antenna feed	55.4	22.7	59.6	+8
Solar panel 1 (1T3) (x right tip)	22.8	20.2	53.1	+133
Solar panel 1 (1C1)	34.2	20.6	54.1	+58
Solar panel 1 (1C2)	45.2	25.4	66.7	+47
Solar panel 1 (1C3)	25.1	21.2	55.7	+122
Solar panel 3 (3T1)	25.6	18.3	48.1	+88
Solar panel 3 (3T3)	43.0	21.6	56.7	+32
Solar panel 7 (7T3)	29.0	23.0	60.4	+108
Low-gain antenna tip (0T1)	74.0	27.6	72.5	−2
Midcourse motor (MC2)	26.6	6.3	16.5	−28
Sun sensor	35.1	32.0	84.0	+140
Plasma probe (PP1)	30.7	19.8	52.0	+69

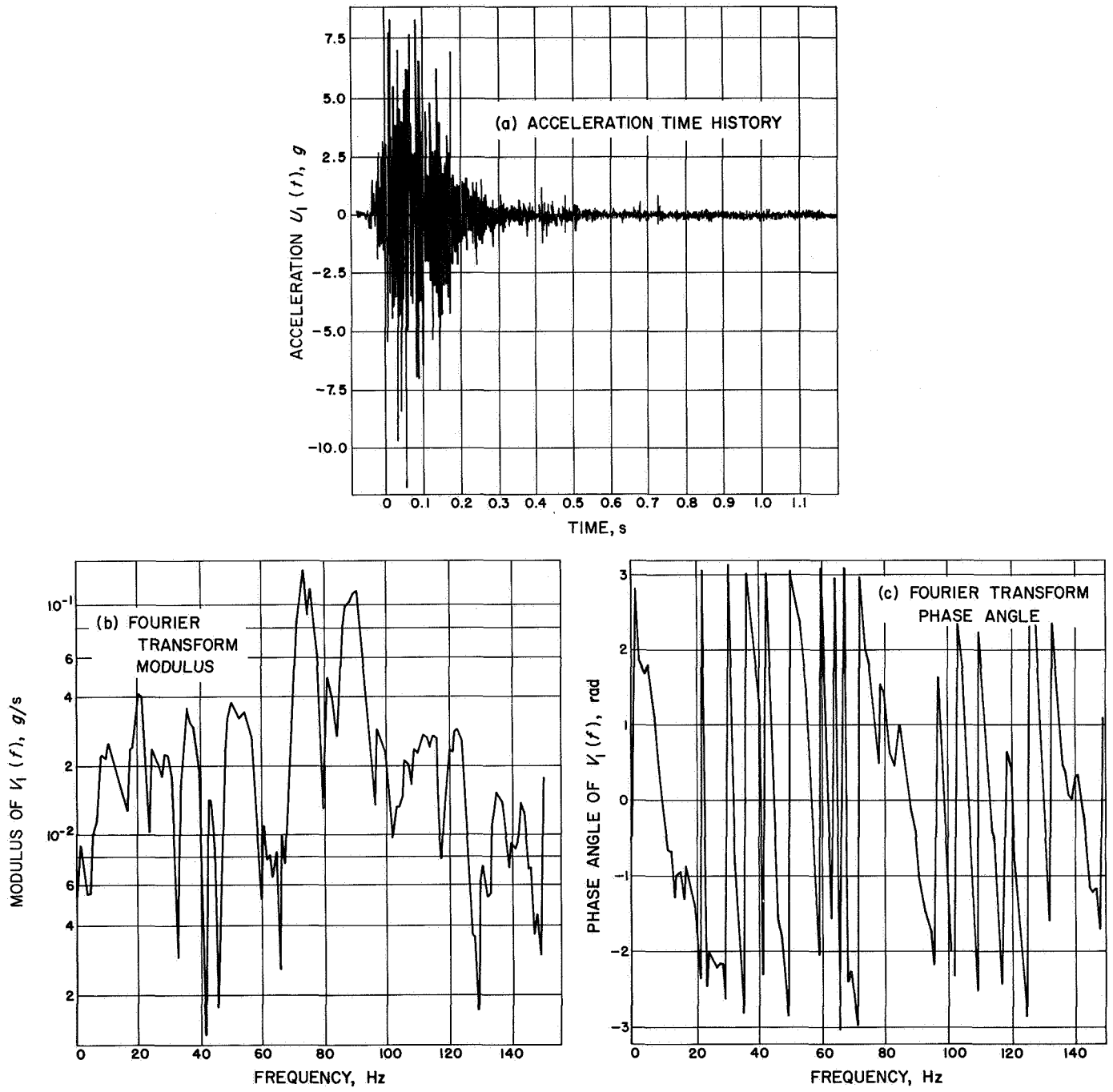

Fig. 18. Response acceleration for solar panel 1, position 1T3, pulse 3 excitation

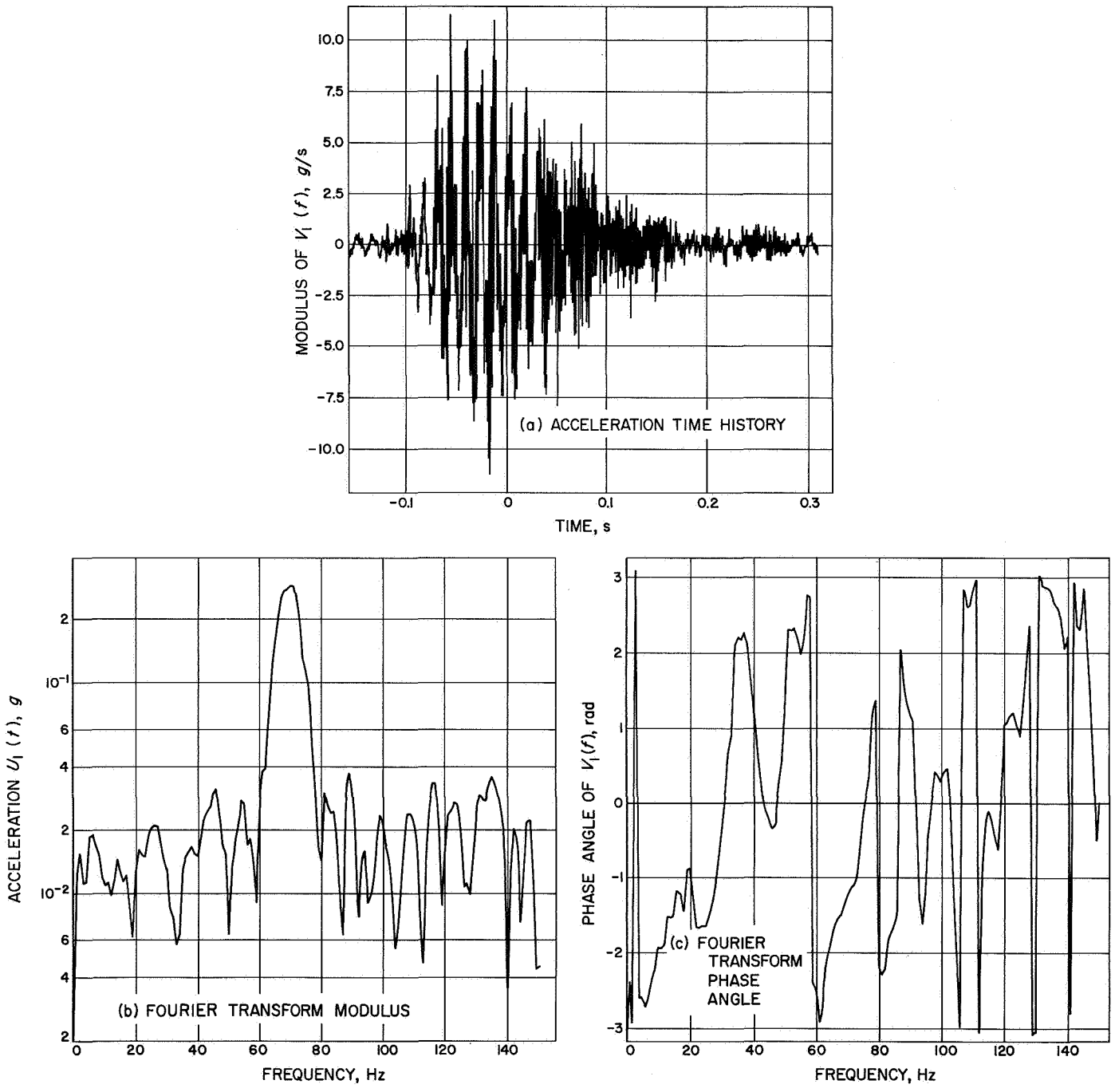

Fig. 19. Response acceleration for solar panel 1, position 1T3, 69-Hz pulse excitation

It is worth noting that the solar panels are more sensitive to the wideband excitation of the multifrequency pulse 3 than other structural elements. For example, the right tip of solar panel 1 exhibited an amplitude that was 133% greater for the multifrequency pulse than it was for the 69-Hz pulse. We also note that, for the location where the 69-Hz pulse gives higher response, it was with a much lower percentage (column 4). There are two possible explanations for the 69-Hz pulse producing more amplitude response for some locations:

(1) No mode of significant amplitude occurs for these locations, with a possible exception of a mode near 69 Hz.

(2) The 69-Hz excitation stays near its maximum level for a relatively long period of time, while the multifrequency pulse only briefly reaches its maximum (Figs. 17 and 20).

Finally, by looking at the Fourier transform of all pulses that have a high response with the multifrequency pulse 3 (mostly solar panels), it can be seen that they all exhibit significant secondary peaks below or above about 70 Hz which do not exist in the base acceleration—showing the influence of several modes below and above 70 Hz.

1. Transfer function. Besides giving a frequency spectrum of the data, the Fourier transform of both the input and output pulses permits the determination of the transfer functions $H(f)$ from the base motion to various points of the responding spacecraft, in which f is the frequency, in Hz.

Let us call $X(f)$ the Fourier transform of the base motion and $Y(f)$ the Fourier transform of the response at one location on the spacecraft; then we have (from Ref. 3):

$$Y(f) = H(f) \quad X(f) \tag{1}$$

$$H(f) = \frac{Y(f)}{X(f)} \tag{2}$$

Equation (2) means that the transfer function is the complex ratio of the Fourier transform of the response to the Fourier transform of the base motion. Figure 20 shows the modulus $H(f)$ and the phase angle θ for one location on the spacecraft where

$$H(f) = (R^2 + I^2)^{1/2} \tag{3}$$

$$\theta = \tan^{-1}\frac{I}{R} \tag{4}$$

$$H(f) = R + jI \tag{5}$$

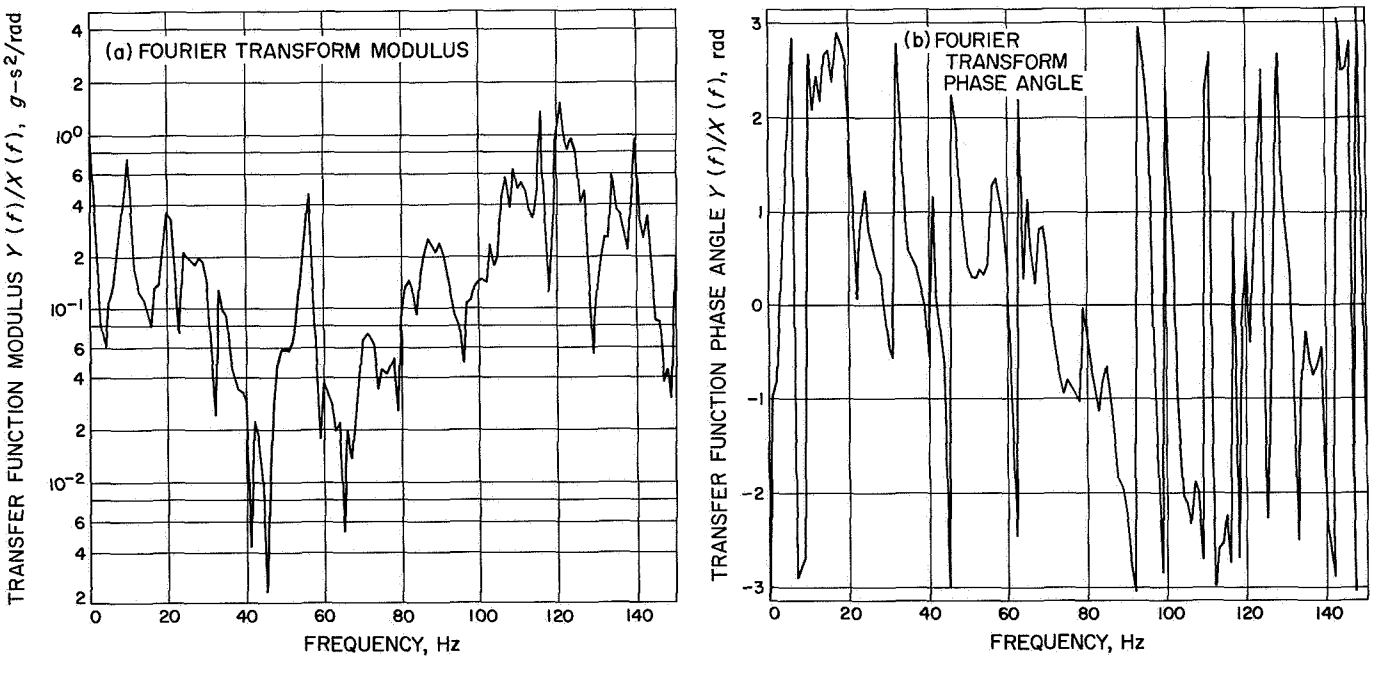

Fig. 20. Transfer function for solar panel 1, position 1T3, pulse 3 excitation

R and I are the real and imaginary parts of the transfer function $H(f)$. The transfer function $H(f)$ is a by-product of the test data. Nevertheless, it is a very valuable quantity, since it characterizes the structure and permits a subsequent computation of the dynamic response of the structure when exposed to any kind of known base acceleration.

2. *Remarks.* Caution must be exercised in the interpretation of the phase angle θ. Proper time correlation between the input pulse and the response pulse must be effective. This time correlation was only roughly maintained during the digitizing process. Indeed, the input and output pulses come from different electromagnetic tape channels and are not digitized simultaneously, but in reference to a common time reference. Therefore, there exists a time difference τ_0 between the origin of the two pulses. The time τ_0 comes from two sources:

(1) From the ability to start digitizing at a prescribed time (The time error can be of the order of 50 μs.)

(2) From the inherent time delay between tracks on the magnetic tape (This time delay depends on the tape heads and should be evaluated for both the data-acquisition tape recorder and the data-reproduction tape recorder. It can be expected to be of the same order as for the above. In any event, this time delay could be measured.)

Concerning the effect on the phase angle of the transfer function, we have (from Ref. 2):

$$\theta = \theta_Y - \theta_X + 2\pi f \tau_0 \tag{6}$$

where

θ_X is the phase angle for $X(f)$

θ_Y is the phase angle for $Y(f)$

The term $2\pi f \tau_0$ is the type of error we can expect to have on the phase angle θ.

IV. Conclusion

The STM successfully demonstrated its ability to withstand structural qualification dynamic loads in the most critical test configuration. It is valid to conclude that, on the basis of these tests, a high degree of confidence exists as to the spacecraft's structural integrity.

The dynamic-response characteristics of the test structure when subjected to qualification-level loads have been well defined. The magnitudes of response are within acceptable limits, and the test structure demonstrated a minimum amount of dynamic coupling. The pressure-sensitive dynamic response of the PIPS and its effect on the spacecraft has been obtained and is well within the design constraints of the overall structure.

Appendix A
Hardware Assemblies Qualified on the STM

1. Octagon structure, including miscellaneous mounting brackets
2. Bay II shear web
3. Temperature control louvers
4. Upper thermal blanket
5. Lower thermal blanket
6. Deployable sunshade, including deployment hardware
7. Fixed sunshades
8. Side thermal shields
9. Temperature control references
10. Solar panel structures
11. Separation-initiated timer
12. Pyro arming switch
13. Upper ring harnesses (9W1 and 9W2) and cable-trough structure
14. Lower ring harness (9W19)
15. Squib firing harnesses (9W8, 9W28, 9W38)
16. PIPS wiring harnesses (9W10 and 9W11)
17. Superstructure
18. High-gain antenna structure
19. High-gain antenna deployment hardware, including deploy switch
20. PIPS support structure and adjustment pads
21. Sun sensor pedestal (Bays II and VI)
22. Umbilical connector bracket
23. Plasma support bracket
24. Trapped radiation detector support bracket
25. Dual frequency receiver antennas
26. Attitude control jet sun shade
27. Low-gain antenna structure
28. Low-gain antenna dampers
29. Solar-panel boost dampers
30. Solar-panel deploy springs and switches
31. Solar-panel cruise damper and latch assemblies
32. Science signal harnesses (9W22, 9W24, 9W26)
33. Magnetometer coaxial cables (9W29 and 9W34)

Appendix B
Instrumentation Run Sheets

Table B-1. *Mariner V* STM vibration test[a] (June 15, 1966)

No.	General location	Component code	Instrument-sensitive direction	Accelerometer type	Magnetic tape, multiplex position
1	Input control	1	In direction of excitation	2272	1
2	Input control	2	In direction of excitation	2272	2
3	Input control	3	In direction of excitation	2272	3
4	Input control	4	In direction of excitation	2272	4
5	Input control	5	In direction of excitation	2272	5
6	Input control	6	In direction of excitation	2272	6
7	Flight position bus	B3	z	2217	7
8	Top of bus, leg F	B4	x	2221	8
9	Top of bus, leg F	B5	y	2221	9
10	Top of bus, leg F	B6	z	2221	10
11	Top of bus, leg D	B9	x	2221	11
12	Top of bus, leg D	B10	y	2221	12
13	Top of bus, leg D	B11	z	2221	13
14	Adapter, spacecraft/booster	F1	Radial at foot G	2213	14
15	Adapter, spacecraft/booster	F3	Tangent at foot C	2213	15
16	Adapter, spacecraft/booster	F4	z	2217	16
17	Secondary structure	SS1	z	2228	17
18	Secondary structure	SS2	In line bays IV-VIII	2228	18
19	Secondary structure	SS3	In line bays II-VI	2228	19
20	Secondary structure	SS4	z	2228	20
21	Secondary structure	SS5	In line bays IV-VIII	2228	21
22	Secondary structure	SS6	In line bays II-VI	2228	22
23	Antenna support structure	AS1	x	2221	23
24	Antenna support structure	AS2	y	2221	24
25	Antenna support structure	AS3	z	2221	25
26	Antenna support structure	AS4	x	2221	26
27	Antenna support structure	AS5	y	2221	27
28	Antenna support structure	AS6	z	2221	28
29	High-gain antenna dish	HG1	Perpendicular at tip	2226	29
30	High-gain antenna feed	HG2	In line bays IV-VIII	2221	30
31	Canopus sensor	CS1	z	2228	31
32	Canopus sensor	CS2	In line bays II-VI	2228	32
33	Canopus sensor	CS3	In line bays IV-VIII	2228	33
34	Canopus sensor	CS4	z	2228	34
35	Canopus sensor	CS5	In line bays II-VI	2228	35
36	Canopus sensor	CS6	In line bays IV-VIII	2228	36
37	Solar panel 1	1T1	x Left tip	2226	37
38	Solar panel 1	1T2	y Left tip	2226	38
39	Solar panel 1	1T3	x Right tip	2226	39
40	Solar panel 1	1M1	x Midpoint	2226	40
41	Solar panel 1	1H1	x Hinge-sliding	2221	41
42	Solar panel 1	1H2	z Hinge-sliding	2221	42
43	Solar panel 1	1H3	x Hinged-fixed	2228	43
44	Solar panel 1	1H4	y Hinge-fixed	2228	44
45	Solar panel 1	1H5	z Hinge-fixed	2228	45
46	Solar panel 1	1C1	x Cell side	CEC MINI	46
47	Solar panel 1	1C2	x Cell side	CEC MINI	47
48	Solar panel 1	1C3	x Cell side	CEC MINI	48

Table B-1 (contd)

No.	General location	Component code	Instrument-sensitive direction	Accelerometer type	Magnetic tape, multiplex position
49	Solar panel 1	1C4	x Cell side	CEC MINI	49
50	Solar panel 3	3T1	y Left tip	2226	50
51	Solar panel 3	3T2	x Left tip	2226	51
52	Solar panel 3	3T3	y Right tip	2226	52
53	Solar panel 3	3M1	y Midpoint	2226	53
54	Solar panel 3	3H1	y Hinge-sliding	2221	54
55	Solar panel 3	3H2	z Hinge-sliding	2221	55
56	Solar panel 3	3H3	y Hinge-fixed	2228	56
57	Solar panel 3	3H4	x Hinge-fixed	2228	57
58	Solar panel 3	3H5	z Hinge-fixed	2228	58
59	Solar panel 5	5T1	x Right tip	2226	59
60	Solar panel 5	5T2	y Right tip	2226	60
61	Solar panel 5	5T3	x Left tip	2226	61
62	Solar panel 7	7T1	y Left tip	2226	62
63	Solar panel 7	7T2	x Left tip	2226	63
64	Solar panel 7	7T3	y Right tip	2226	64
65	Trapped radiation detector	TRD1	In line bays IV-VIII	2221	65
66	Trapped radiation detector	TRD2	In line bays II-VI	2221	66
67	UV photometer	UV1	z	2221	67
68	UV photometer	UV2	In line bays II-VI	2221	68
69	Low-gain antenna tip	0T1	x	2226	69
70	Low-gain antenna tip	0T2	y	2226	70
71	Midcourse motor	MC1	z	2221	71
72	Midcourse motor	MC2	In line bays IV-VIII	2221	72
73	Sun sensor	SUN1	x	2221	73
74	Sun sensor	SUN2	y	2221	74
75	Midcourse motor frame	MC4	In line bays II-VI	2221	75
76	Plasma probe	PP1	z	2221	76
77	Time code				77
78	Sine reference				78
1	Solar panel damper[b]	SG1			1
2	Solar panel damper[b]	SG2			2
3					3
4					4
5					5
6					6
7					7
8					8
9					9
10					10
11					11
12	Time code				12
13	Sine reference				13
14	Voice label				14

[a]Changes to basic instrumentation during testing:

1. Run 58 and remainder. At the request of the Environmental Requirements Section representative, channels 8–9 were switched with channels 13–16. New assignments were: channel 8 to B11; channel 9 to F4; channel 13 to B4; and channel 16 to B5.
2. Run 71 and remainder. Components 1H1, 1H2, 3H1, and 3H2 were disconnected; HG3 and HG4 were added to the spacecraft; and SG1 and SG2 were moved to the multiplex recorder. The following channel assignments were made: channel 41 to HG3; channel 42 to HG4; channel 54 to SG1; and channel 55 to SG2.

[b]Strain gages used for these tests.

Table B-2. STM follow-up vibration test (October 14, 1966)

No.	General location	Component code	Instrument-sensitive direction	Accelerometer type	Magnetic tape, multiplex position
1	Flight position bus	B3	z	2217	1-1
2	Top of bus, leg F	B6	z	2221	1-2
3	Top of bus, leg D	B11	z	2221	1-3
4	Adapter, flight position	F4	z	2217	1-4
5	Module top Bay III	A-1	z	2221	1-5
6	Module middle Bay III	A-2	z	2221	1-6
7	Module bottom Bay III	A-3	z	2221	2-7
8	Adapter, spacecraft/booster	F1	Radial foot G	2213	2-8
9	Adapter, spacecraft/booster	F3	Tangent foot C	2213	2-9
10	Top of bus, leg F	B4	x	2221	2-10
11	Top of bus, leg F	B5	y	2221	2-11
12	Top of bus, leg D	B9	x	2221	2-12
13	Top of bus, leg D	B10	y	2221	3-13
14	Secondary structure	SS1	z	2228	3-14
15	Secondary structure	SS2	In line bays IV-VIII	2228	3-15
16	Secondary structure	SS3	In line bays II-VI	2228	3-16
17	Secondary structure	SS4	z	2228	3-17
18	Secondary structure	SS5	In line bays IV-VIII	2228	3-18
19	Secondary structure	SS6	In line bays II-VI	2228	4-19
20	Antenna support structure	AS-1	Parallel to antenna	2221	4-20
21	Antenna support structure	AS-2	Normal to antenna	2221	4-21
22	Antenna support structure	AS-4	Parallel to antenna	2221	4-22
23	Antenna support structure	AS-5	Normal to antenna	2221	4-23
24	High-gain antenna dish	HG-1	Normal at tip	2226	4-24
25	High-gain antenna feed	HG-2	In line bays IV-VIII	2221	5-25
26	High-gain antenna feed	HG-3	In line bays II-VI	2221	5-26
27	High-gain antenna feed	HG-4	z	2221	5-27
28	Canopus sensor	CS1	z	2228	5-28
29	Canopus sensor	CS2	In line bays II-VI	2228	5-29
30	Canopus sensor	CS3	In line bays IV-VIII	2228	5-30
31	Canopus sensor	CS4	z	2228	6-31
32	Canopus sensor	CS5	In line bays II-VI	2228	6-32
33	Canopus sensor	CS6	In line bays IV-VIII	2228	6-33
34	Trapped radiation detector	TRD1	In line bays IV-VIII	2221	6-34
35	Trapped radiation detector	TRD2	In line bays II-VI	2221	6-35
36	UV photometer	UV1	z	2221	6-36
37	UV photometer	UV2	In line bays II-VI	2221	7-37
38	Low-gain antenna tip	0T1	x	2226	7-38
39	Low-gain antenna tip	0T2	y	2226	7-39
40	Midcourse motor	MC1	z	2221	7-40
41	Midcourse motor	MC2	In line bays IV-VIII	2221	7-41
42	Midcourse motor frame	MC4	In line bays II-VI	2221	7-42
43	Midcourse motor	MC1A	z	2221	8-43
44	Sun sensor	SUN2	y	2221	8-44
45	Plasma probe	PP1	z	2221	8-45
46	Solar panel 1	1T1	x Left tip	2226	8-46
47	Solar panel 1	1T2	y Left tip	2226	8-47

Table B-2 (contd)

No.	General location	Component code	Instrument-sensitive direction	Accelerometer type	Magnetic tape, multiplex position
48	Solar panel 1	1T3	x Right tip	2226	8-48
49	Solar panel 1	1TCR	x Input to TCR[b]	2226	9-49
50	Solar panel 1	1H3	x Hinge fixed	2228	9-50
51	Solar panel 1	1H4	y Hinge fixed	2228	9-51
52	Solar panel 1	1H5	z Hinge fixed	2228	9-52
53	Solar panel 1	1C1	x Cell side	CEC MINI	9-53
54	Solar panel 1	1C2	x Cell side	CEC MINI	9-54
55	Solar panel 1	1C3	x Cell side	CEC MINI	10-55
56	Solar panel 1	1C4	x Cell side	CEC MINI	10-56
57	Solar panel 3	3T1	y Left tip	2226	10-57
58	Solar panel 3	3T2	x Left tip	2226	10-58
59	Solar panel 3	3T3	y Right tip	2226	10-59
60	Solar panel 3	3H3	y Hinge fixed	2228	10-60
61	Solar panel 3	3H4	x Hinge fixed	2228	11-61
62	Solar panel 3	3H5	z Hinge fixed	2228	11-62
63	Solar panel 5	5T1	x Right tip	2226	11-63
64	Solar panel 5	5T2	y Right tip	2226	11-64
65	Solar panel 5	5T3	x Left tip	2226	11-65
66	Solar panel 7	7T1	y Left tip	2226	11-66
67	Solar panel 7	7T2	x Left tip	2226	12-67
68	Solar panel 7	7T3	y Right tip	2226	12-68
69	Solar panel damper[a]	SG1	Right panel 1		12-69
70	Solar panel damper[a]	SG2	Right panel 3		12-70
71	Time code				12-71
72	Sine reference				12-72
	Input control	1	In direction of excitation	2272	13-73
	Input control	2	In direction of excitation	2272	13-74
	Input control	3	In direction of excitation	2272	13-75
	Input control	4	In direction of excitation	2272	13-76
	Input control	5	In direction of excitation	2272	13-77
	Input control	6	In direction of excitation	2272	13-78
	Track 14 voice label				

[a]Strain gages were used for these channels.
[b]Temperature control reference.

Appendix C

Torsional Transient Loads Analysis

The philosophy used for the derivation of the torsional transients to be applied at the base of the *Mariner* Venus 67 STM is similar to the one presented in Ref. 1 for *Surveyor*. However, the method used here was different in its application, as explained in Ref. 2. In brief, in Ref. 1 use is made of a time-domain solution, while in

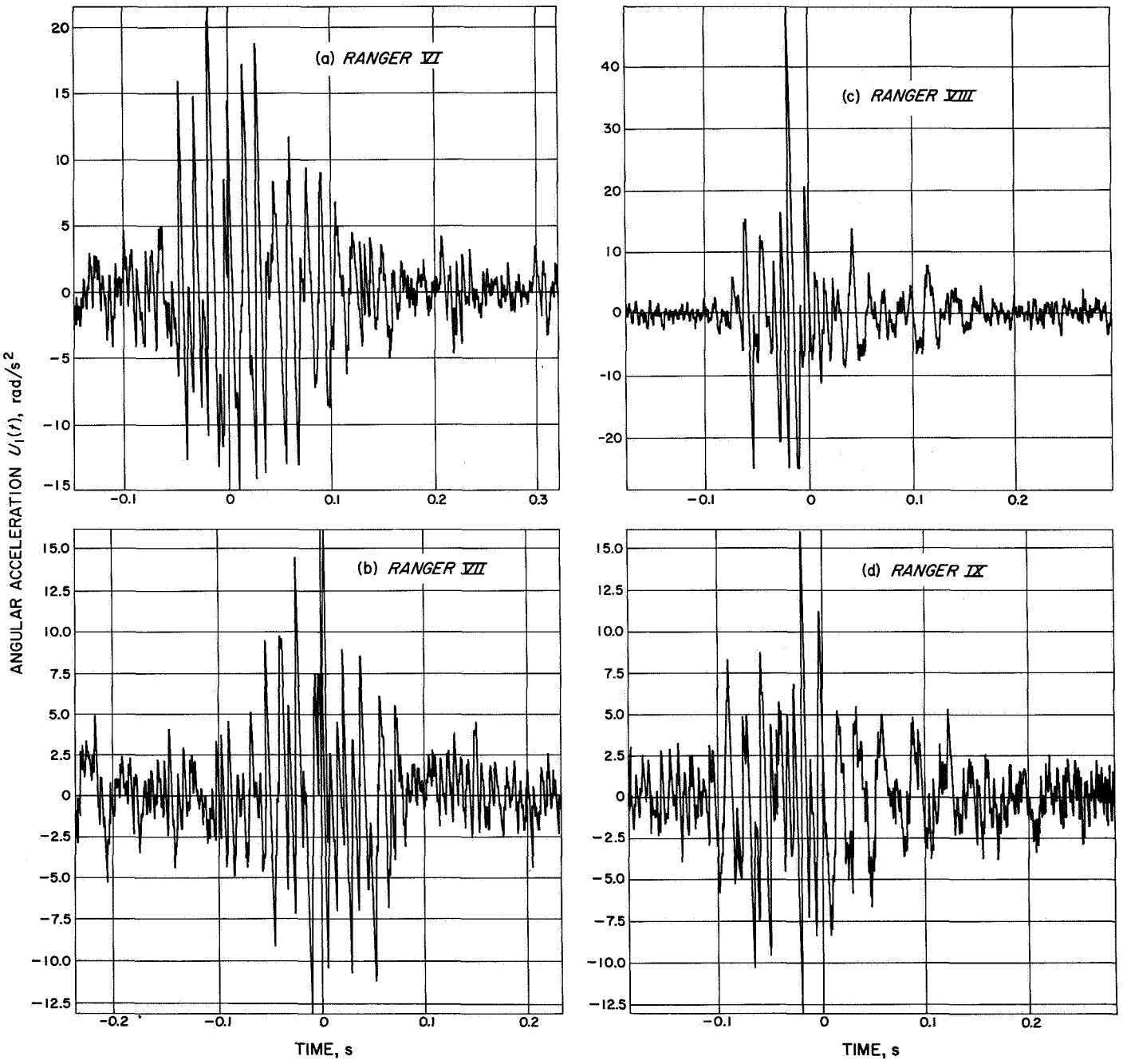

Fig. C-1. *Ranger* torsional-transient-flight acceleration time histories

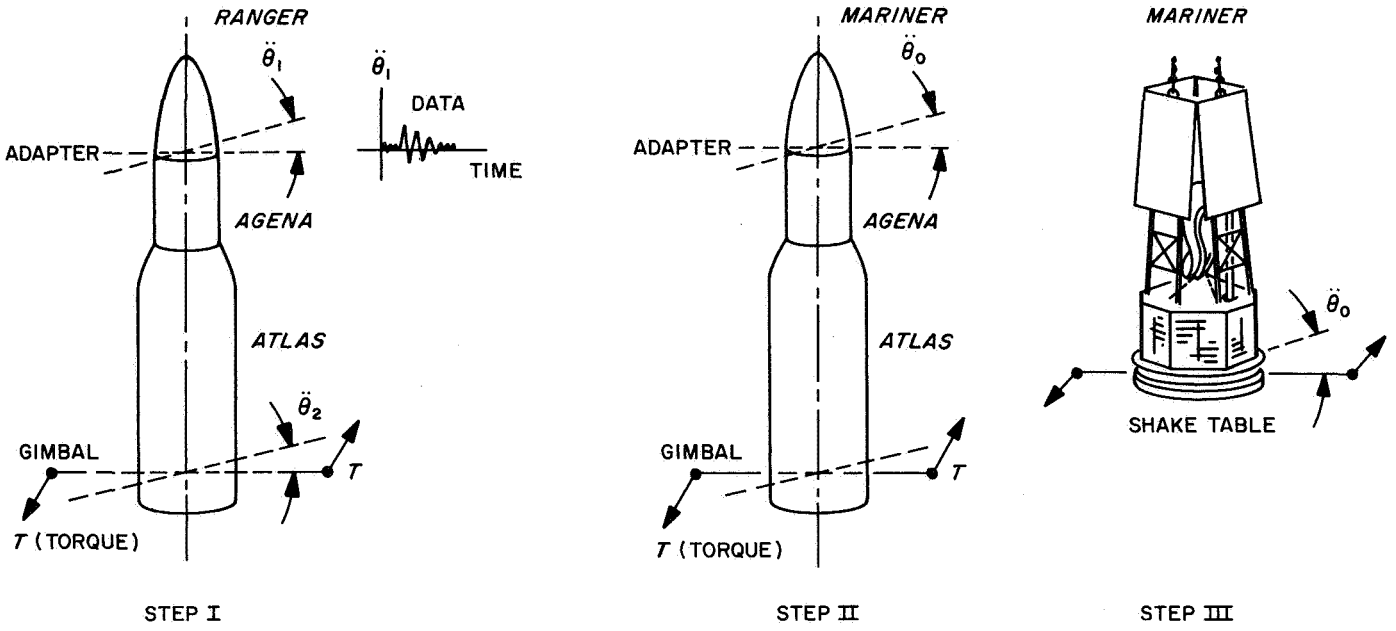

Fig. C-2. *Mariner* Venus 67 torsional loads analysis and torsional test

Ref. 2 a frequency-domain solution is employed with Fourier transform technique; the latter was found to be more rational and less costly.

Step 1. Booster engine cutoff (BECO) torsional flight acceleration data of *Rangers VI* and *IX* were used (Fig. C-1), and it was assumed that this acceleration was due to a torque T (t) applied at the gimbal blocks of the *Atlas* engine at BECO (see Fig. C-2). This unknown torque T (t) was deduced from the flight data using a mathematical model to represent the *Atlas/Agena–Ranger* vehicle in torsion.

Step 2. Because both spacecraft, the *Ranger* and the *Mariner*, use the same *Atlas* booster, it was assumed that the same character of disturbance would occur for the *Mariner* flight, inducing a torsional transient at the base of the spacecraft. Therefore, the torque T (t) deduced in step 1 was applied to the mathematical model of the *Atlas/Agena–Mariner* vehicle, and the spacecraft base acceleration was deduced. To account for uncertainties, the level of these pulses was multiplied by a factor of 2 to obtain the qualification testing level. Figures C-3 through C-6 (time history and Fourier transforms) show the four qualification-level pulses that were applied at the base of the spacecraft for the torsional pulse test.

Step 3. For the vibration test, a magnetic tape was prepared that gave the voltage-time history to be applied at the shaker coils to reproduce the desired base acceleration transients. To this end, an analog computer was used which represented the electromechanical characteristics of the shaker system, together with the mass, elastic, and damping properties of the spacecraft. The method used to prepare this tape was completely identical to the one presented in the first JPL specification cited in footnote 1 (p. 1).

Figures C-7 through C-10 show the time histories and their Fourier transforms of the four pulses that were obtained during the actual test by playing the magnetic tape prepared in step 3. By comparison to the time histories and Fourier transforms of the acceleration requirements (Figs. C-3 through C-6), it can be seen that the levels and frequency distribution were satisfactorily reproduced on the shake table.

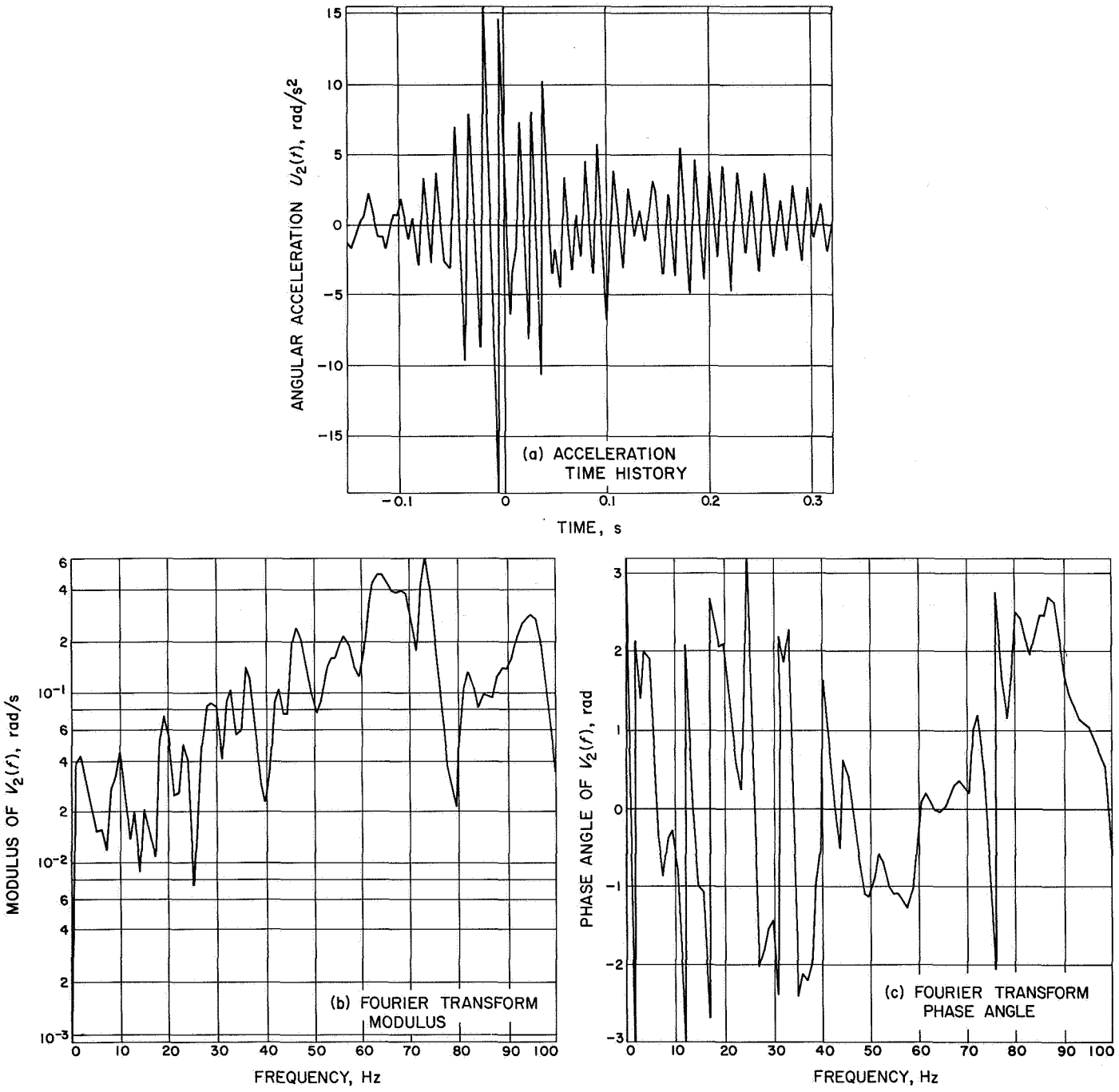

Fig. C-3. *Mariner* Venus 67 torsional acceleration test requirement, pulse 1

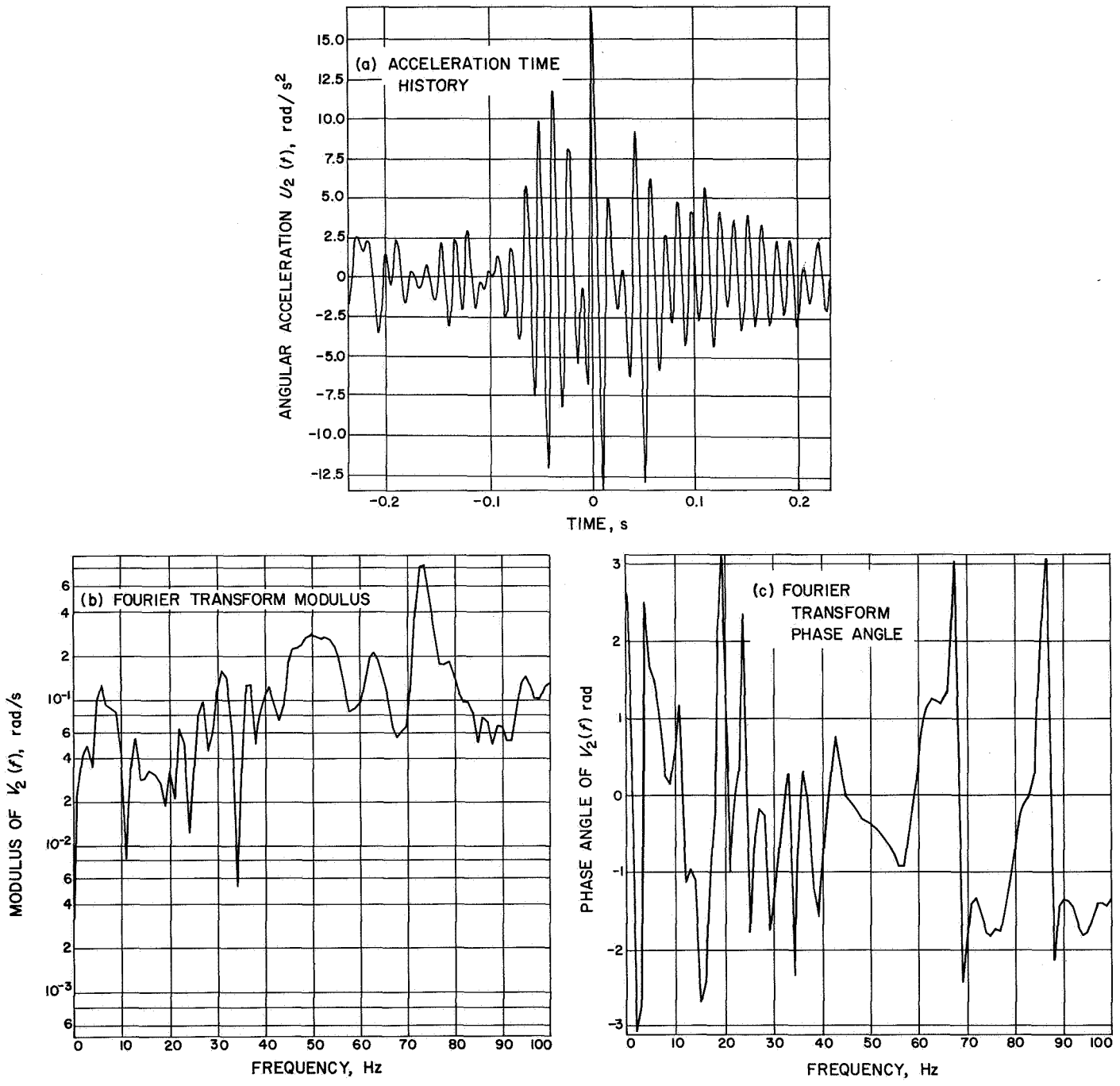

Fig. C-4. *Mariner* Venus 67 torsional acceleration test requirement, pulse 2

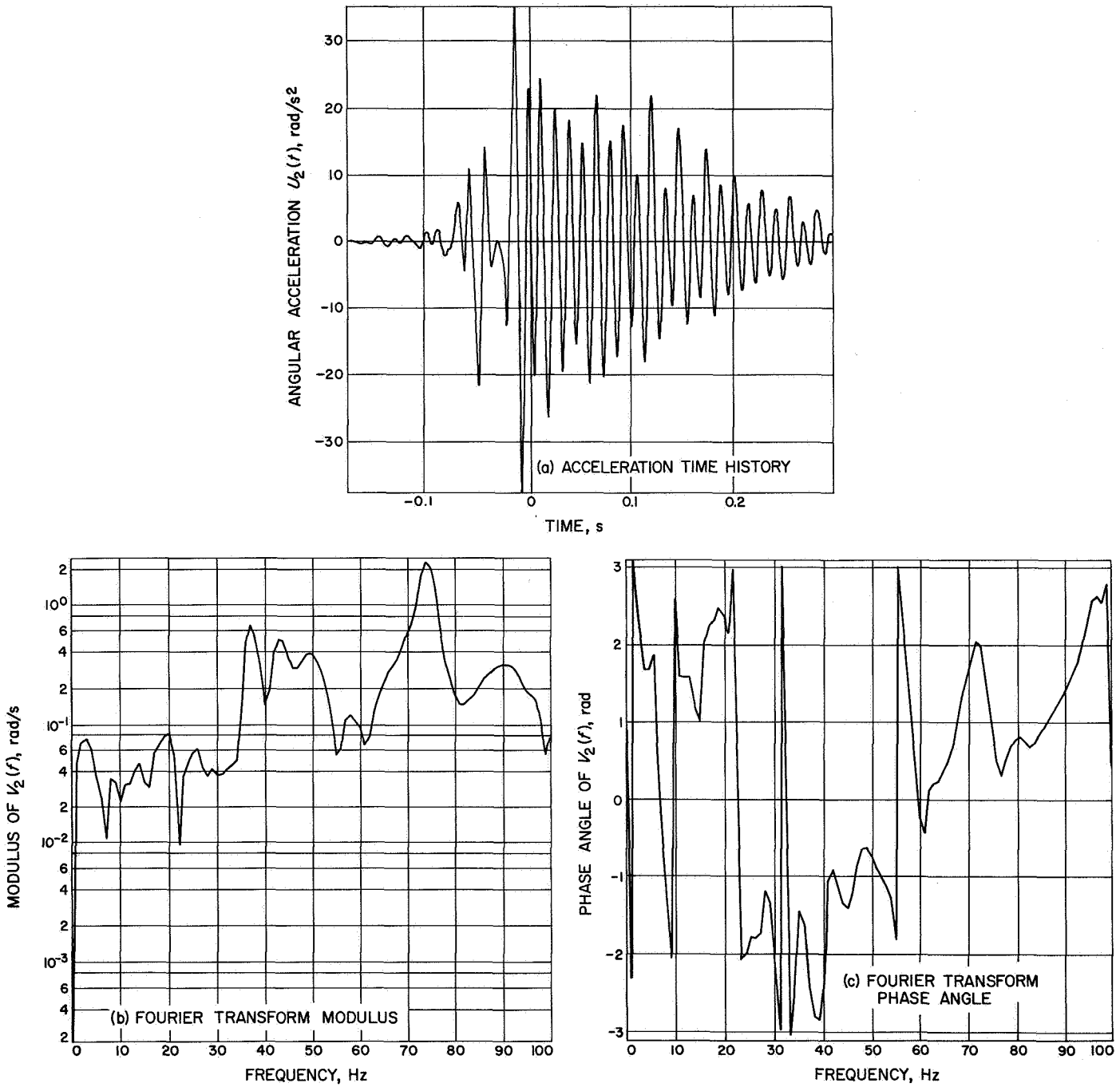

Fig. C-5. *Mariner* Venus 67 torsional acceleration test requirement, pulse 3

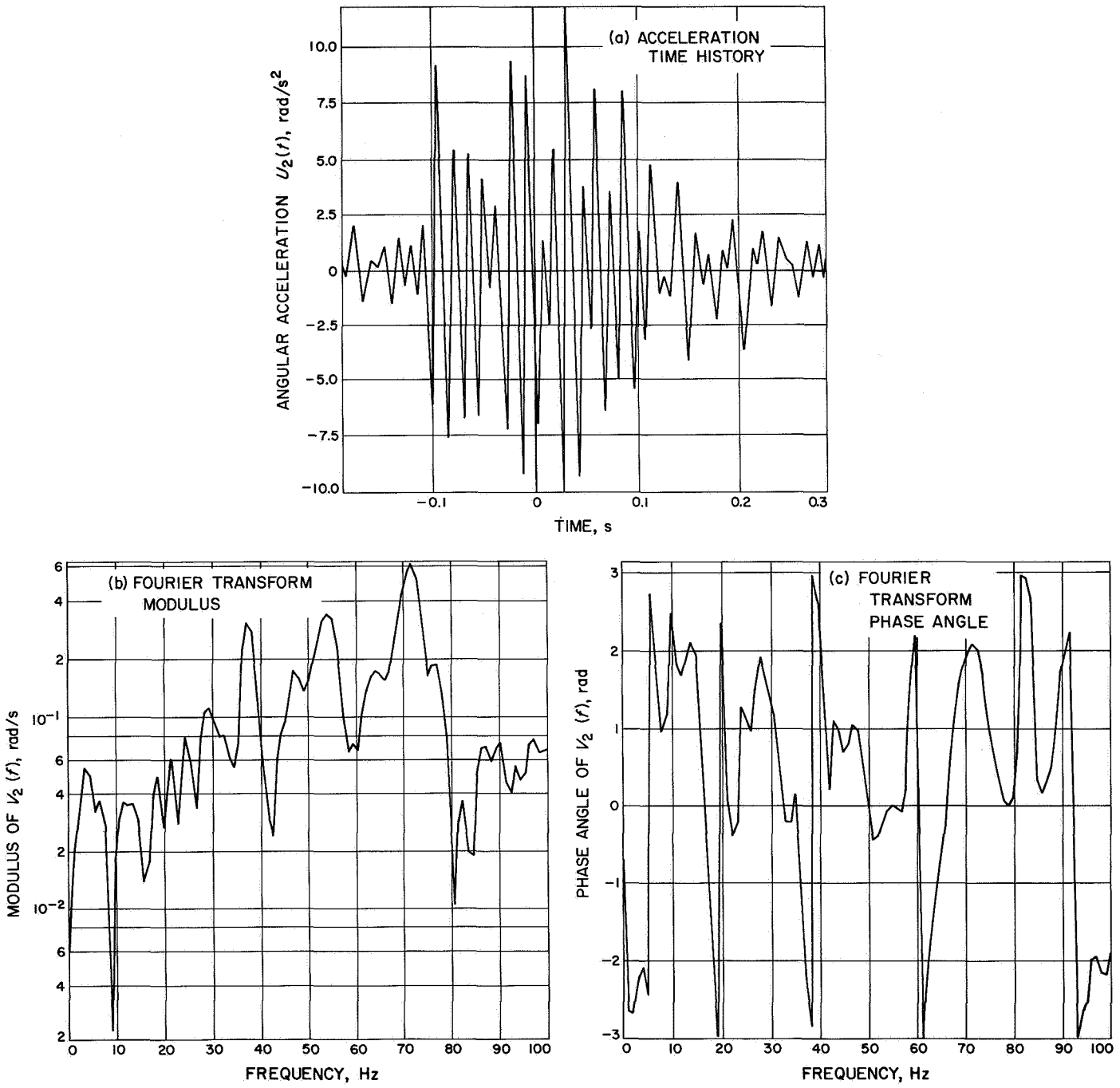

Fig. C-6. *Mariner* Venus 67 torsional acceleration test requirement, pulse 4

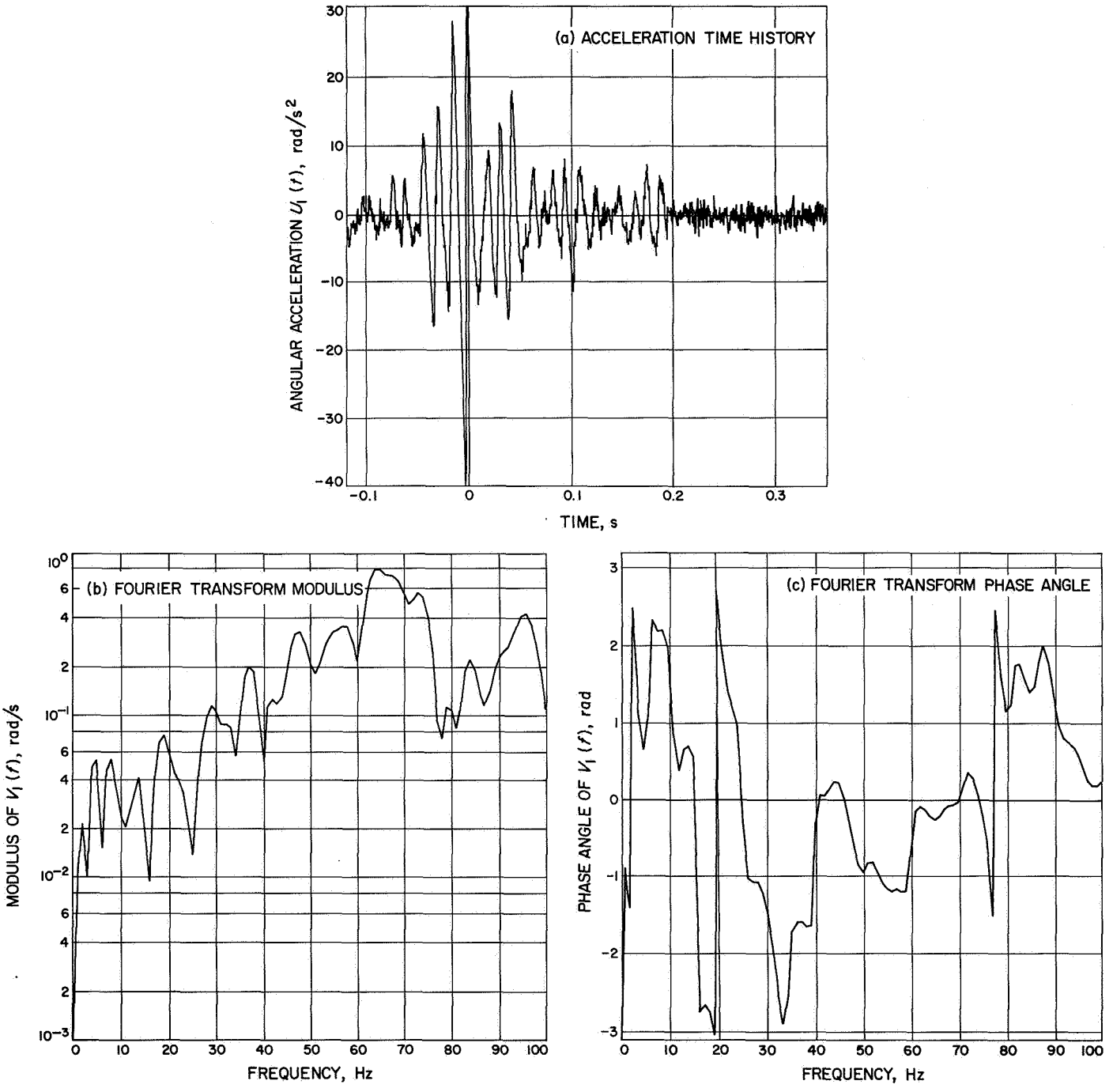

Fig. C-7. Actual STM torsional acceleration, pulse 1

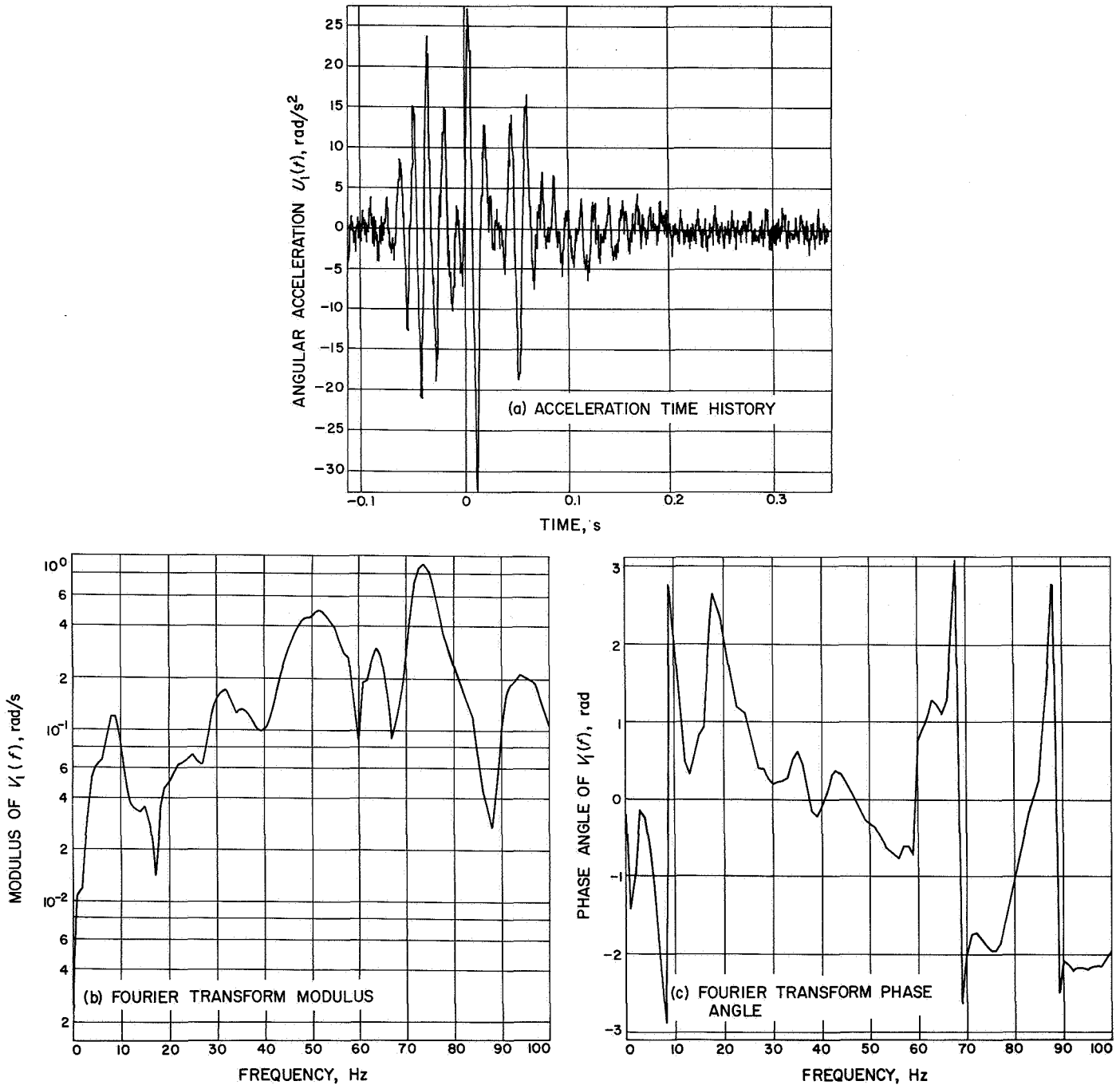

Fig. C-8. Actual STM torsional acceleration, pulse 2

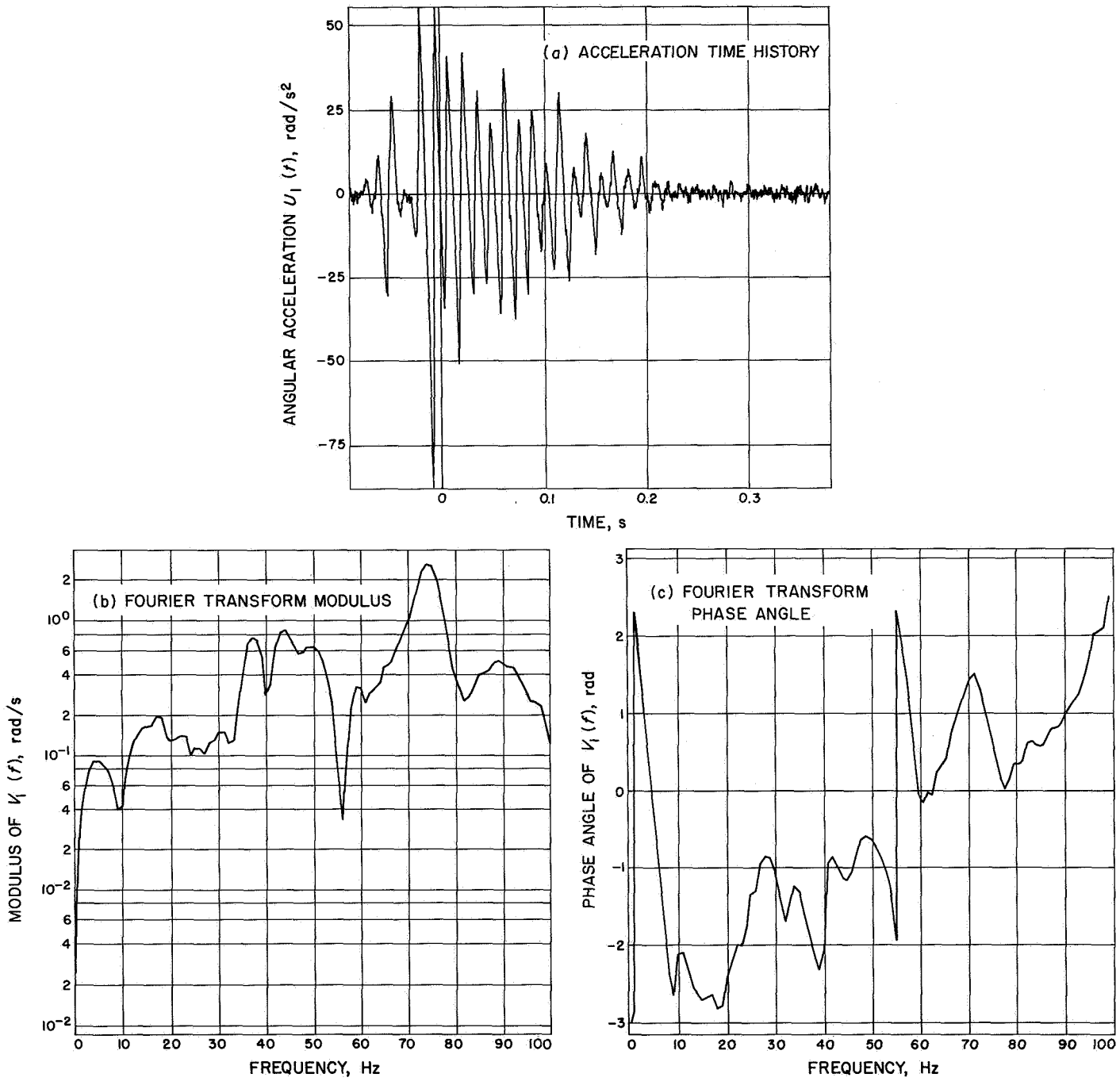

Fig. C-9. Actual STM torsional acceleration, pulse 3

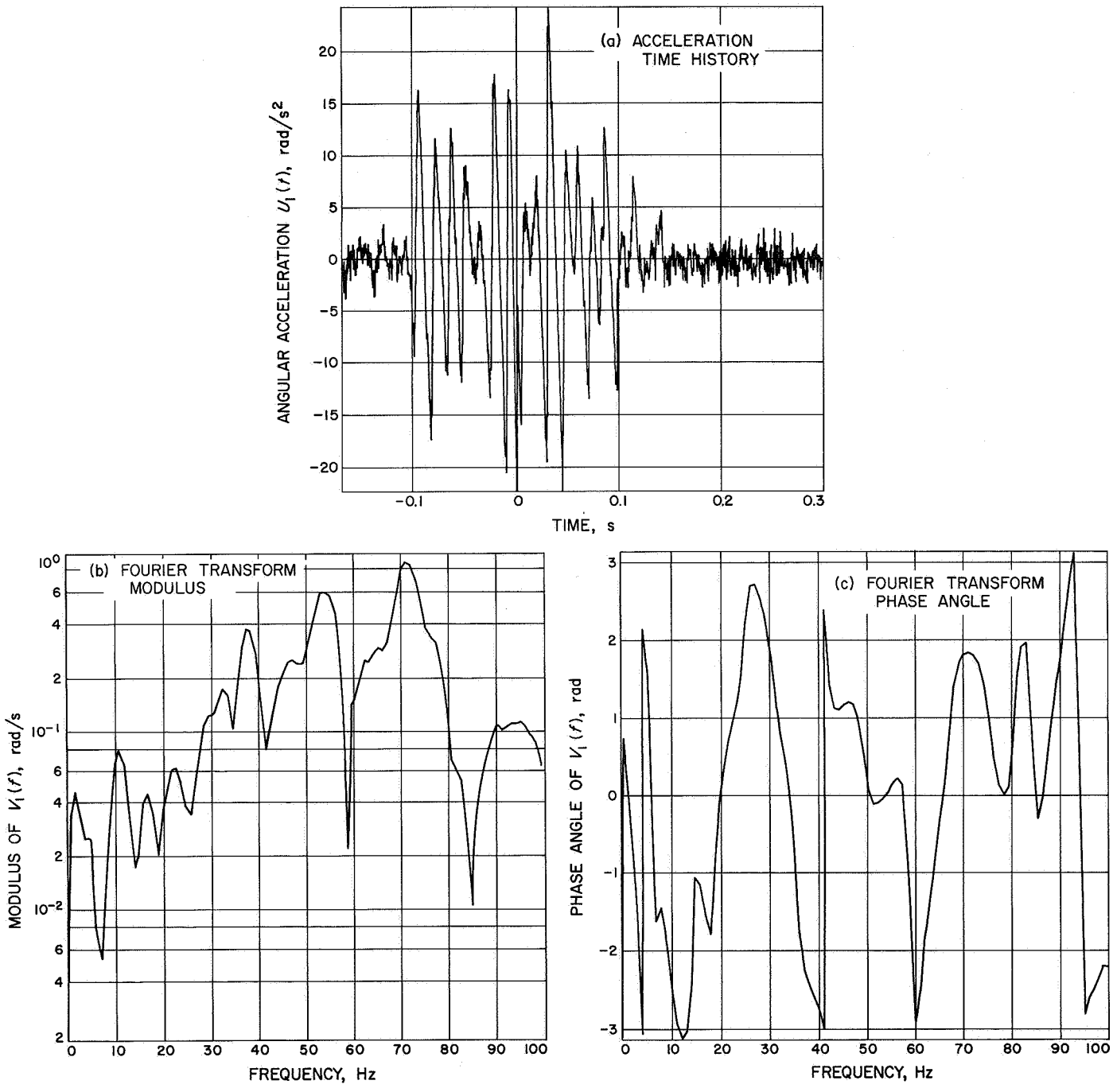

Fig. C-10. Actual STM torsional acceleration, pulse 4

References

1. Trubert, M. R., *Use of Ranger Flight Data in the Synthesis of a Torsional Acceleration Transient for Surveyor Vibration Qualification Testing,* Technical Memorandum No. 33-737, Jet Propulsion Laboratory, Pasadena, Calif., April 19, 1966.
2. Trubert, M. R., *A Fourier Transform Technique for the Prediction of Torsional Transients for a Spacecraft From the Flight Data of Another Spacecraft Using the Same Booster,* Technical Memorandum 33-350, Jet Propulsion Laboratory, Pasadena, Calif., Oct. 15, 1967.
3. Crandall, S. H., and Mark, W. D., *Random Vibration in Mechanical Systems,* p. 57, Academic Press, New York, 1963.